MICROARRAY TIME COURSE ASSAYS OF CHO-CELLS IMPALED ON VERTICALLY ARRAYED NANOFIBERS

By

SEBASTIAN M. HARRIS

Bachelor of Science in Chemistry

Southwestern Oklahoma State University

Weatherford, OK

2007

Submitted to the Faculty of the
Graduate College of the
Oklahoma State University
in partial fulfillment of
the requirements for
the Degree of
MASTER OF SCIENCE
December, 2009

MICROARRAY TIME COURSE ASSAYS OF CHO-

CELLS IMPALED ON VERTICALLY ARRAYED

NANOFIBERS

Thesis Approved:

Dr. Peter Hoyt

Thesis Adviser

Dr. Robert Matts

Dr. Ramanjulu Sunkar

Dr. Gordon Emslie

Dean of the Graduate College

ACKNOWLEDGMENTS

I would like to graciously thank Dr. Peter Hoyt for accepting me into his lab and for his guidance and support. I would also like to thank the entire Department of Biochemistry and Molecular Biology at Oklahoma State University for their support. Finally, I would like to thank my family and friends for keeping me going even in the most difficult times.

TABLE OF CONTENTS

LIST OF FIGURES

CHAPTER I

INTRODUCTION

The integrity of the cellular plasma membrane is essential for maintaining viability of any eukaryotic cell. The extent of a rupture in the plasma membrane can result in rapid lysis of the cell, or a survival mechanism successfully repairs damage to the plasma membrane and reestablishes homeostasis in the cell with respect to the environment [1]. The latter outcome has been the focus of many research programs because the inability for cells to repair their plasma membrane has been linked to human diseases such as heart failure and neurodegeneration[1-4]. The disease state is a consequence of poor membrane repair or accelerated death of irreplaceable cell types. Unfortunately, the mechanism by which the cell responds to an injury to the cell membrane is still quite elusive but some clues have been revealed. Previous studies have shown that intracellular vesicles in organelle containing cells are delivered to the site of damage on the plasma membrane. Entry of extracellular Calcium after plasma membrane rupture induces a membrane repair signal and aids in the fusion of the intracellular vesicles to the plasma membrane [5-8]. Deployment of these intracellular vesicles has been shown to involve rearrangement of microtubules toward the site of membrane damage [9].

This study describes the cellular response to a novel wounding caused by impalement and permanent residency of nanofibers in living cells. This type of wounding has not been studied at the level of transcriptome. The goal of this project was to determine whether the healing response would resolve sufficiently such that new genetic perturbations could be introduced and studied in live, impaled cells. We hypothesize that some common mechanisms will be identified when impaled cells are compared to known mechanisms of plasma membrane repair. This study

is important because the interfacing of live cells with nano-electromaterials has the potential to provide an active protective barrier for medicinal implants to regulate gliotic scarring, and provide extended life to implants modulating disease progression.

Mechanisms for Plasma Membrane Repair

One model for resealing a rupture in the plasma membrane is the plasma membrane itself. Cells are known to maintain relatively low intracellular Calcium levels. Maintenance of Calcium is essential for normal cell functioning as Calcium is a widely utilized signaling molecule in metabolism. In the absence of Calcium, isolated liposomes will reseal after small ruptures are induced without contributions from additional organelles. Also red blood cells (RBCs) do not contain organelles but will reseal a rupture in the membrane when low extracellular Calcium is present [10]. Even nucleated cells with a small rupture (<1 um) have been shown to reseal in the absence of Calcium [11]. Thus a self-sealing mechanism is proposed to be driven by increase of free energy from the disordering of the ordered acyl chains within the phospholipid bilayer surrounding the membrane rupture. However, these observations were made under a controlled environment and have not been observed under physiological conditions. When a RBC lyses, the cytoskeleton is observed to breakdown with an increasing influx of Calcium leading to accelerated alteration of the phospholipid bilayer [11,12]. The high influx of Calcium is proposed to prevent any thermodynamically favorable resealing of cell membrane. Together these observations demonstrate that low extracellular levels Calcium can aid in resealing a rupture in the plasma membrane but if a rupture allows intracellular Calcium influx to reach extracellular, physiologic levels, it is usually lethal to the integrity of the cell.

The first models discussed revealed lines of evidence that the plasma membrane can reseal spontaneously under the specific conditions. A plausible model has been proposed in which membrane damage causes the cell to actively provide intracellular vesicles as an organized response to membrane wounding, and to counter unfavorable environments[13]. The reasoning behind this model is that high membrane tension (tensile force along the membrane) has been shown in fibroblasts to prevent resealing due to counteracting the free energy of local lipid disorder. The production and release of free vesicles from the Golgi apparatus to the wound site has been correlated with reduction of membrane tension thus allowing resealing to occur [13,14,15]. Although it has been determined that this type of organized cell repair is found in multiple cell types, the type of vesicles or other aiding factors varies. For example. lysosomes and enlargosomes are two of the most prominent vesicles in CHO cells that have been directly shown to fuse to the plasma membrane at the site of injury after an influx of extracellular Calcium.[15]

Nanofibers

A novel method has been developed in the field of carbon based nanofiber synthesis resulting in vertically aligned carbon nanofibers (VACNF). The synthesis of VACNFs consists of many precisely controlled stages. First, is preparation of thin film islands of catalyst material by means of physical vapor deposition through lithographically patterned resist masks. Next the catalyst film is pretreated by increasing the temperature of the film through substrate, laser irradiation, or ion irradiation and placed in a reducing atmosphere of hydrogen gas or plasma. This pretreatment results in dewetting of the film and formation of catalyst nanoparticles. Now the last step is the growth of the nanofiber from the base of the catalyst nanoparticle. This last step is achieved by introduction of a carbonaceous gas over the film. Carbon layers continually

deposit underneath the catalyst nanoparticle allowing the catalyst nanoparticle to rise on top and the nanofiber to elongate. These steps have been improved upon to create whole arrays of VACNFs. [16]

These VACNFs have been in development for biological application with recent studies utilizing VACNFs as a method of cell impalement and transfection [16.] Furthermore, the length and spacing of the nanofibers has been optimized for cell impalement and maintaining cell viability. For "impalefection", attachment of a Green Fluorescent Protein (GFP) encoding plasmid to the nanofiber is transfected into the impaled cells. Figure 1 and Figure 2 clearly demonstrate growth and attempts at motility of live cells following impalement and transfection of GFP[16].

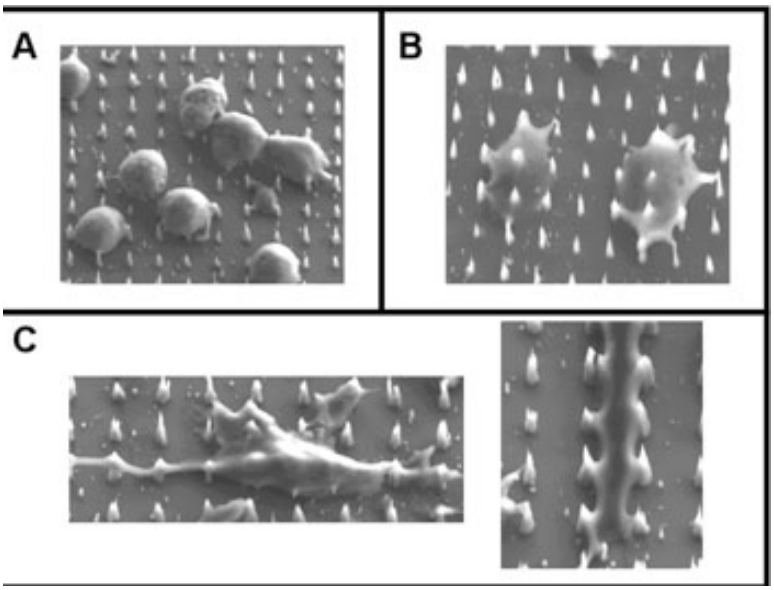

Figure 1. Scanning electron micrographs of cells following (A) centrifugation, (B) press, and (C) culture for 48 h (scale bars = 10 μm). Reproduced with permission from Dr. Timothy McKnight, Oak Ridge National Laboratory. [17]

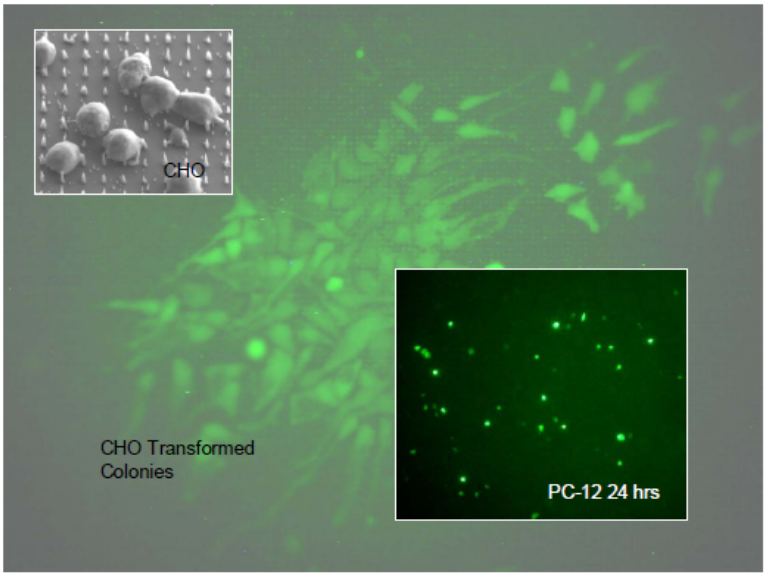

Figure 2: Impalement of CHO and PC-12 cells with GFP expression vector modified VACNFs. The success of impalement is demonstrated by the expression of green fluorescent protein. Reproduced with permission from Dr. Timothy McKnight, Oak Ridge National Laboratory. [16]

CHAPTER II

METHODOLOGY

Nanofiber and Cell Impalement

VACNF arrays were synthesized according to McKnight, T. E. et al. The cell line used for these experiments was the Chinese hamster ovary (CHO). Cells were grown in Ham's F-12 nutrient mixture supplemented with 1 mM glutamine and 5% fetal bovine serum. Cell cultures were grown in T-75 Flasks. Once the culture has a desired density ranging from 50 000 to 600 000 cells ml−1, the CHO cells were centrifuged at 600 G out of suspension onto these chips, which resulted in some cellular impalement on VACNFs. Optionally, to increase the probability

and depth of fiber penetration into cells, the chip was then gently pressed against a flat, wetted surface following the spin (Figure 3). Another set of chips were used as controls with the CHO cells seeded on the nanofiber chip with no impalement application. Following these integration steps, the chips were placed in growth media in a culture dish and incubated with a set of impaled and seeded chips removed at 30, 60, 120, and 240 minutes and 24 hours and placed at -20C in RNA Later.

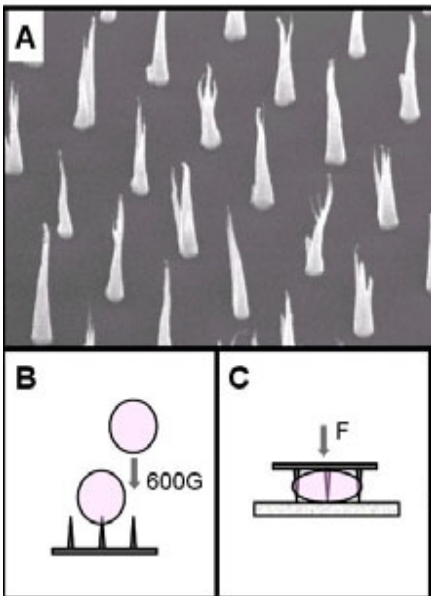

Figure 3: A) Scanning electron micrograph of a carbon nanofiber array lithographically defined with 5 um spaced, 7 um tall fibers with tip diameters of 30 nm. Scale bar = 5 μm. B) Cells are spun out onto a VACNF. C) Following the spin, the substrate may be pressed against a wetted, flat surface. Reproduced with permission from Dr. Timothy McKnight, Oak Ridge National Laboratory. [17]

Beadmilling and RNA Isolation

Nanochips with CHO cells either impaled or seeded from each time point were removed from RNA Later and placed in 1.5ml screw cap microfuge tubes already containing seven, 3mm

silica beads from Biospec (Bartlesville, OK) and ~1ml of solution containing 2.9 mM Guanidium Thiocyanate, 18.1 mM Citric Acid pH=7.0, 0.36% N-Lauryl Sarcosine, and 19.8 nM Beta-mercaptoethanol (BME) that was made using diethyl pyrocarbonate treated water (DEPC-H2O) and filtered with 0.22 um nylon membrane. A Beadbeater from Biospec ™ (Bartlesville, OK) in combination with the small beads and the Guanidium buffer was used to break open the cells and shear the DNA. To prevent overheating, the tubes were treated to one minute of beadmilling followed by thirty seconds of cooling in an ice water bath. This alternation between shearing and cooling was repeated at least eight times. To each tube 95% ethanol was added in an amount that corresponded to 50% of the volume of the extract in the tube, bringing the final EtOH concentration to 33%. The combined mixture was transferred to RNA purification columns (RNeasy Mini kit, QIAGEN™ , cat # 74104) for isolation of total RNA.

Amplification

The Epicentre ™ 2-Round amino-allyl (aa)-RNA Amplification kit was utilized to amplify antisense RNA according to the manufacturers instructions. This amplification method allows the indirect incorporation of fluors by incorporating reactive amino-allyl UTP into RNA during the amplification process. A starting amount of 50pg-500pg of RNA isolate was used for each time point and replicate. The amount of aa-UTP used in the reaction mix in the second round of amplification was optimized to three-times the recommended amount to improve nucleotide to dye ratios in the final labeled target. The yield from amplification was determined using an ND-1000 Spectrophotometer (Nanodrop ™, Inc.) and typically 20-30ug of amino-allyl UTP-labeled antisense.

The amino-allyl UTP in the amplified aRNA was then coupled to NHS-ester-derivitized Cy5 or Cy3 fluors using 100mM Carbonate buffer or a proprietary coupling buffer and protocol from Ambion ™ (Austin, TX). Uncoupled fluors were removed by passing through a cleanup column from a RNeasy Mini kit from QIAGEN™ (cat # 74104). The concentration and nt/dye ratio of the sample was then measured on a NanoDrop ™, ND-1000 spectrophotometer. The optimal conditions for microarray hybridization using Phalanx OneArray ™ Mouse microarrays (described below) was 2ug of labeled anti-sense RNA with a ratio of less than 75 nucleotides per molecule of fluorescent dye incorporated.

Microarray Hybridization

The pre-printed, (>31, 000 features) Phalanx ™ mouse microarray slides were pre-treated by humidifying overnight at 80% humidity. After humidifying, the slides were dried in an oven at 65°C for one hour and then agitated in 95% ethanol for 10-15 minutes. The aaRNA dye coupled samples were hybridized to Phalanx mouse microarray slides utilizing provided protocol version 3.3. No other changes were made to the Phalanx protocol.

Data Analysis

Statistical treatment of raw microarray data was done using Omicsoft ™ Array Studio version 3.0 (Morrisville, NC) (http://www.omicsoft.com/). Microarray data were normalized using quantile normalization and then transformed based on log2 scale. Gene lists were generated using statistical limitations on fold change in gene expression, and confidence p-values. These sets of gene lists were used for functional annotation. Gene Ontology is the classification of genes based on three primary categories: Cellular Component-breakdown of

association and location; Molecular Function-describes a specific activity (ex. Ion exchange); Biological Process-an event that occurs through the grouping of genes with particular molecular functions (ex. Signal transduction). There are many GO subcategories pertaining to the primary three. The gene lists were analyzed for function patterns using the Web Gestalt Gene Ontology (GO) Tree (http://bioinfo.vanderbilt.edu/gotm/) bioinformatics program from Vanderbilt University. Web Gestalt identifies genes significantly over-represented in specific GO categories, and displays them in visually simple GO-Trees where over-represented gene sets are colored in red and given probability assignments. . GO categories were studied for over representation of any subcategories in the form of pie charts using Genesis from the Graz University of Technology (http://genome.tugraz.at/). Finally, KEGG pathway maps from the Kanehisa Laboratories (http://www.genome.jp/kegg) were used to map up and down regulated genes from the gene lists.

CHAPTER III

FINDINGS

Significant Differential Gene Expression is Eliminated by 24 hours

Our data shows that the overall cellular response to nanofiber impalement is largely resolved by 24 hours post-impalement. Studies on membrane repair mechanisms clearly show that calcium influx initiates a wound-repair response [5-8]. Although nanofiber impaled cells have a resident nanofiber "plugging" the membrane wound, it is likely nanofiber penetration would result in variable degrees of calcium influx. Our data supports a model of calcium influx when the overall chaotic response is considered. Calcium initiates and propagates a large number of signal transduction pathways, activates transcription factors and enzymes, and generates an ionic

gradient repair response [19]. At early time points, specific effects of a resident nanofiber cannot be discriminated from this presumptive response to calcium influx.

Impaled cells demonstrated an increase of total differential gene expression peaking at 60 to 120 minutes following impalement. Analysis of total gene expression (Figure 4), statistically significant differential expression using Web Gestalt (Figure 5), and metabolic KEGG pathway maps (Figure 6) demonstrate that by 24 hours the differential expression profile coincides closely with the non impaled control cells. In Figure 4 all valid differentially expressed genes (those passing the statistical criteria for intensity signal mean +/- 1 standard deviation) were compared using thresholding. The trend line in Figure 4 illustrates that first differential gene expression peaks at around 60 to 120 minutes and before it is greatly reduced by 24 hours.

In Figure 5 only genes with a fold change of 0.1 to -0.1 and p-value of 0.3 were compared using Web Gestalt. GO categories highlighted in red are considered significant based on thresholding standards applied. Lines connecting GO categories indicate are part of a hierarchal related classification. In Figure 5 the plots show increases in total differential expression activity (based on the number of red highlighted GO categories) starting at 30 minutes (Figure 5a) and peaking at 120 minutes (Figure 5c) followed by a decreasing trend at 240 minutes (Figure 5d) and a collapse in significant differential gene expression by 24 hours (Figure 5e). Other notable observations were made including the GO categories “plasma membrane” and “protein binding” which were over-represented from 30 to 240 minutes (Figure 5a-d). The GO terms “developmental process” and “multicellular organismal process” are also continually over-represented from 30 minutes to 240 minutes (Figure 5a-d), and an increasing

number of their subcategories are significantly overrepresented peaking at 120 minutes (Figure 5c1-3). One other general GO term “cell communication” and corresponding subcategories appears at 60 minutes until 240 minutes (Figure 5b-d).

Further validation that cells have recovered from impalement by 24 hours is shown using KEGG metabolic pathway maps (Figure 6). These pathway maps show differential activity is severely reduced by 24 hours, suggesting that the cell transcriptome is returning to normal. Metabolic pathway maps represent only a fraction of the known metabolism within cells, but provide an overall view of the cellular activity related to known functions. These pathway maps were generated using a gene list with statistical threshold of 0.1 to -0.1 fold change and 0.3 p-value. These relatively “relaxed” statistical conditions were used because the purpose was to demonstrate that differential gene expression was decreased to near normal, and because the use of hamster RNA with mouse microarray probes increased the probability of false negatives over false positives. Up-regulation is represented by a bold red line and down-regulation by a bold light green. Specific metabolism pathways consistently differentially expressed either up or down until 24 hours include Glycan metabolism, Nucleotide metabolism, Amino Acid metabolism, Lipid metabolism, pentose phosphate pathway, and oxidative phosphorylation.

a)

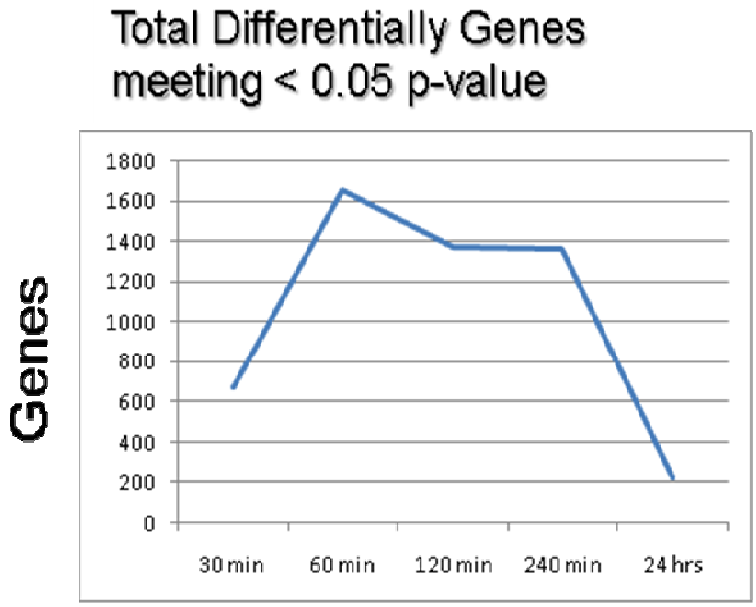

b)

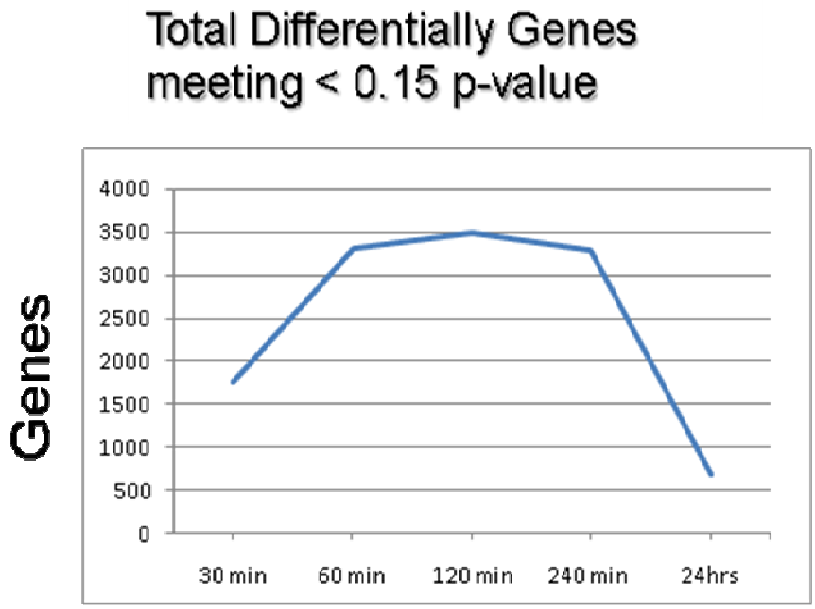

Figure 4: a) Gene list per time point was generated after normalization and transformation with a statistical threshold of 0.1 to -0.1 estimate range and 0.05 p-value. b) Gene list per time point was generated after normalization and transformation with a statistical threshold of 0.1 to -0.1 estimate range and 0.15 p-value.

a)

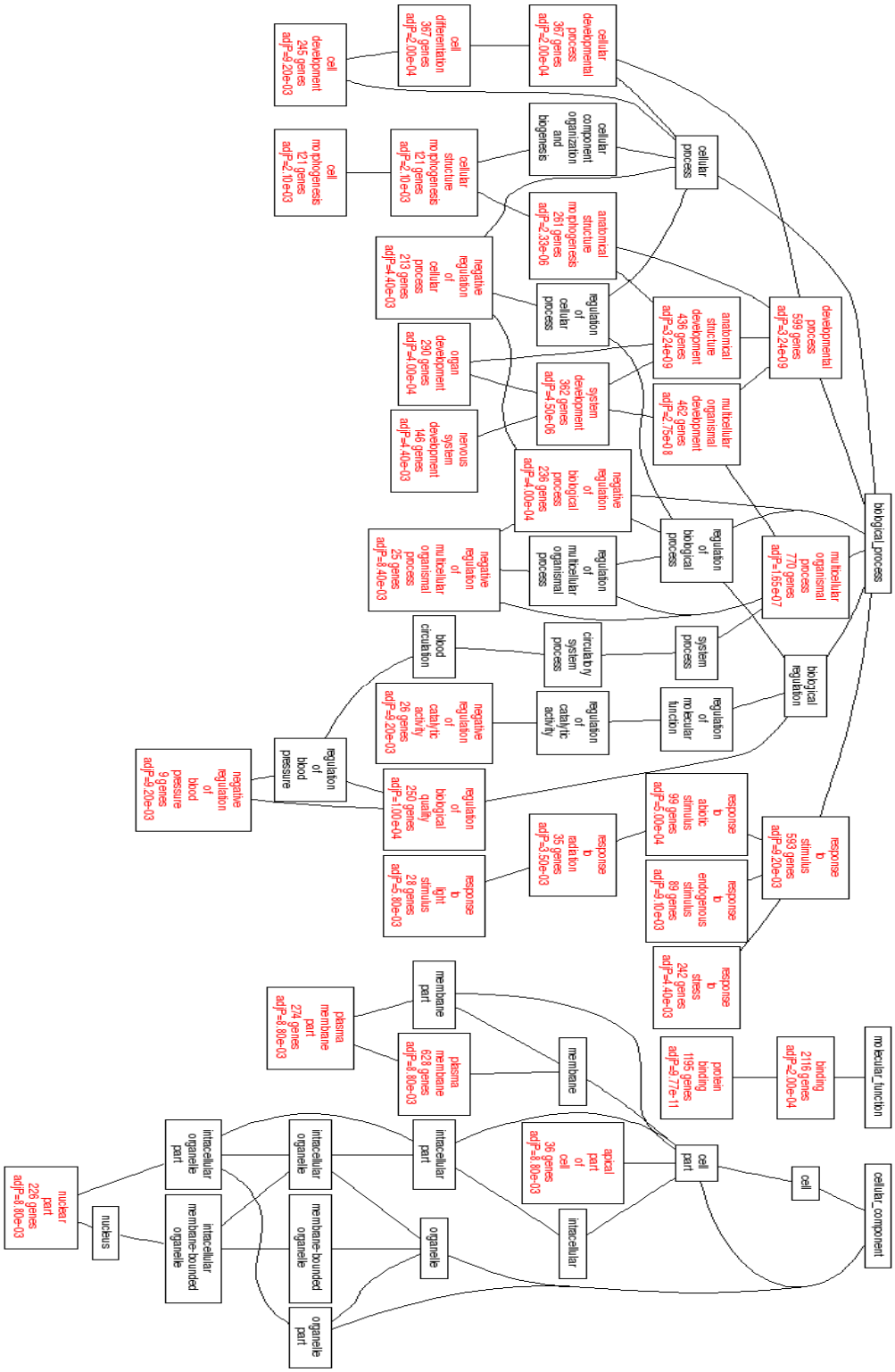
biological_process
developmental process 599 genes adjP=3.24e-09
cellular developmental process 387 genes adjP=2.00e-04
cell differentiation 367 genes adjP=2.00e-04
cell development 245 genes adjP=4.20e-03
anatomical structure development 436 genes adjP=3.24e-09
multicellular organismal development 462 genes adjP=2.75e-08
anatomical structure morphogenesis 261 genes adjP=2.33e-06
cellular component organization and biogenesis
cellular structure morphogenesis 121 genes adjP=2.10e-03
cell morphogenesis 121 genes adjP=2.10e-03
system development 382 genes adjP=4.50e-06
organ development 290 genes adjP=4.00e-04
nervous system development 146 genes adjP=4.40e-03
multicellular organismal process 770 genes adjP=1.65e-07
negative regulation of biological process 236 genes adjP=4.00e-04
regulation of biological process
negative regulation of multicellular organismal process 25 genes adjP=8.40e-03
regulation of multicellular organismal process
biological regulation
circulatory system process
system process
blood circulation
regulation of molecular function
negative regulation of catalytic activity 26 genes adjP=9.20e-03
regulation of catalytic activity
regulation of blood pressure
negative regulation of blood pressure 9 genes adjP=9.20e-03
response to stimulus 593 genes adjP=9.20e-03
response to abiotic stimulus 99 genes adjP=5.00e-04
response to endogenous stimulus 89 genes adjP=9.10e-03
response to stress 242 genes adjP=4.40e-03
regulation of biological quality 250 genes adjP=1.00e-04
response to radiation 35 genes adjP=3.50e-03
response to light stimulus 28 genes adjP=5.80e-03
molecular_function
binding 2116 genes adjP=2.00e-04
protein binding 1195 genes adjP=9.77e-11
membrane part
plasma membrane part 274 genes adjP=8.80e-03
plasma membrane part 628 genes adjP=8.80e-03
membrane
cellular_component
cell
cell part
apical part of cell 36 genes adjP=8.80e-03
intracellular part
intracellular
intracellular organelle
intracellular membrane-bounded organelle
organelle
organelle part
nucleus
nucleus part 226 genes adjP=8.80e-03

b)

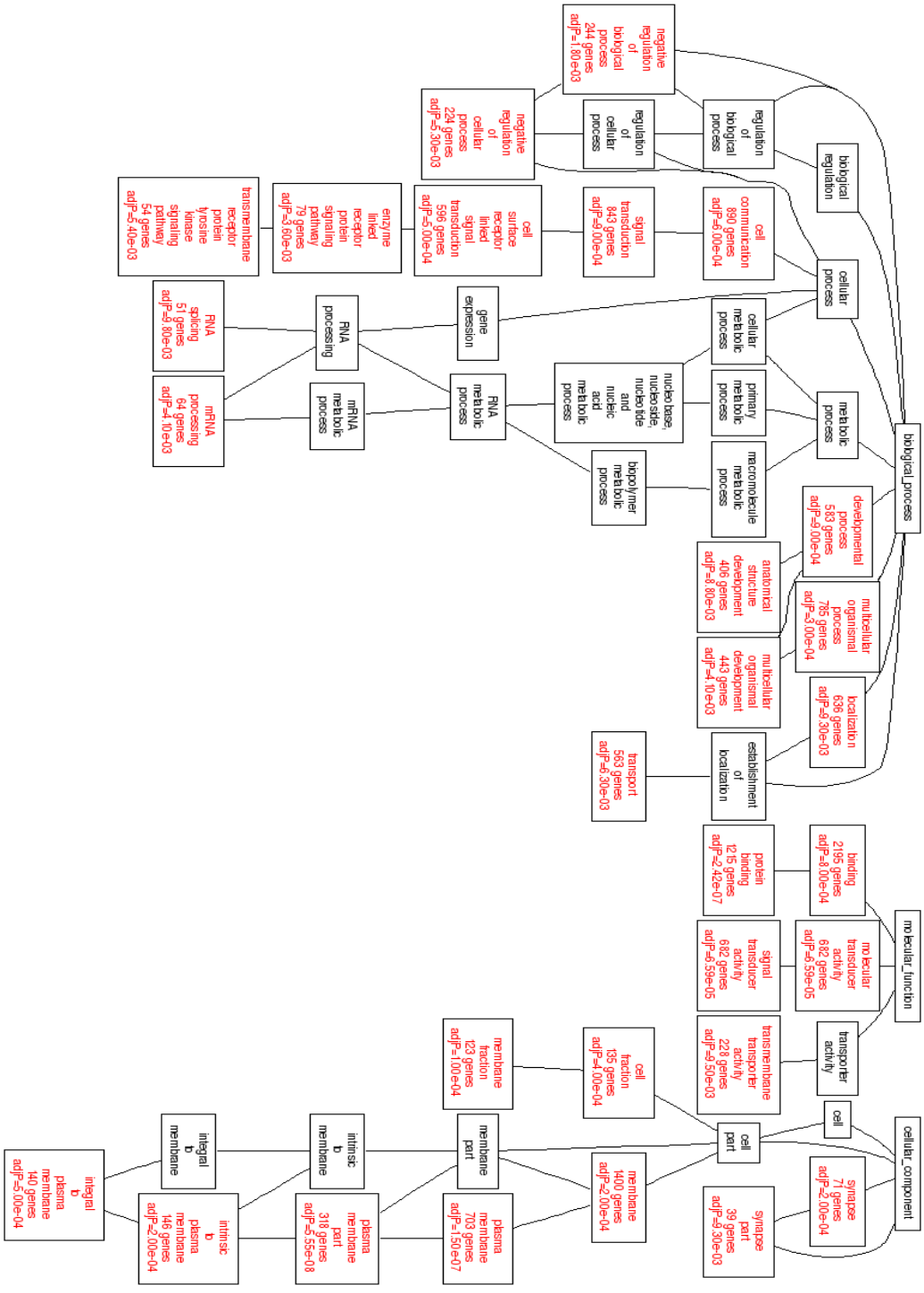
biological_process
molecular_function
cellular_component
biological regulation
cellular process
metabolic process
developmental process
583 genes
adjP=9.00e-04
multicellular organismal process
785 genes
adjP=3.00e-04
localization
636 genes
adjP=9.30e-03
establishment of localization
transport
563 genes
adjP=6.30e-03
anatomical structure development
406 genes
adjP=8.80e-03
multicellular organismal development
443 genes
adjP=4.10e-03
regulation of biological process
negative regulation of biological process
244 genes
adjP=1.80e-03
regulation of cellular process
negative regulation of cellular process
224 genes
adjP=5.30e-03
cell communication
890 genes
adjP=6.00e-04
signal transduction
843 genes
adjP=9.00e-04
cell surface receptor linked signal transduction
596 genes
adjP=3.00e-04
enzyme linked receptor protein signaling pathway
79 genes
adjP=3.60e-03
transmembrane receptor protein tyrosine kinase signaling pathway
54 genes
adjP=5.40e-03
gene expression
cellular metabolic process
primary metabolic process
nucleobase, nucleoside, nucleotide and nucleic acid metabolic process
macromolecule metabolic process
biopolymer metabolic process
RNA metabolic process
RNA processing
RNA splicing
51 genes
adjP=8.80e-03
mRNA metabolic process
mRNA processing
64 genes
adjP=4.10e-03
binding
2195 genes
adjP=8.00e-04
protein binding
1215 genes
adjP=2.42e-07
molecular transducer activity
682 genes
adjP=6.59e-05
signal transducer activity
682 genes
adjP=6.59e-05
transporter activity
transmembrane transporter activity
228 genes
adjP=9.50e-03
cell
cell part
cell fraction
135 genes
adjP=4.00e-04
membrane fraction
123 genes
adjP=1.00e-04
membrane part
membrane
1400 genes
adjP=2.00e-04
plasma membrane part
703 genes
adjP=1.50e-07
intrinsic to membrane
plasma membrane part
318 genes
adjP=5.55e-08
integral to membrane
intrinsic to plasma membrane
146 genes
adjP=2.00e-04
integral to plasma membrane
140 genes
adjP=5.00e-04
synapse
71 genes
adjP=2.00e-04
synapse part
39 genes
adjP=9.30e-03

c1)

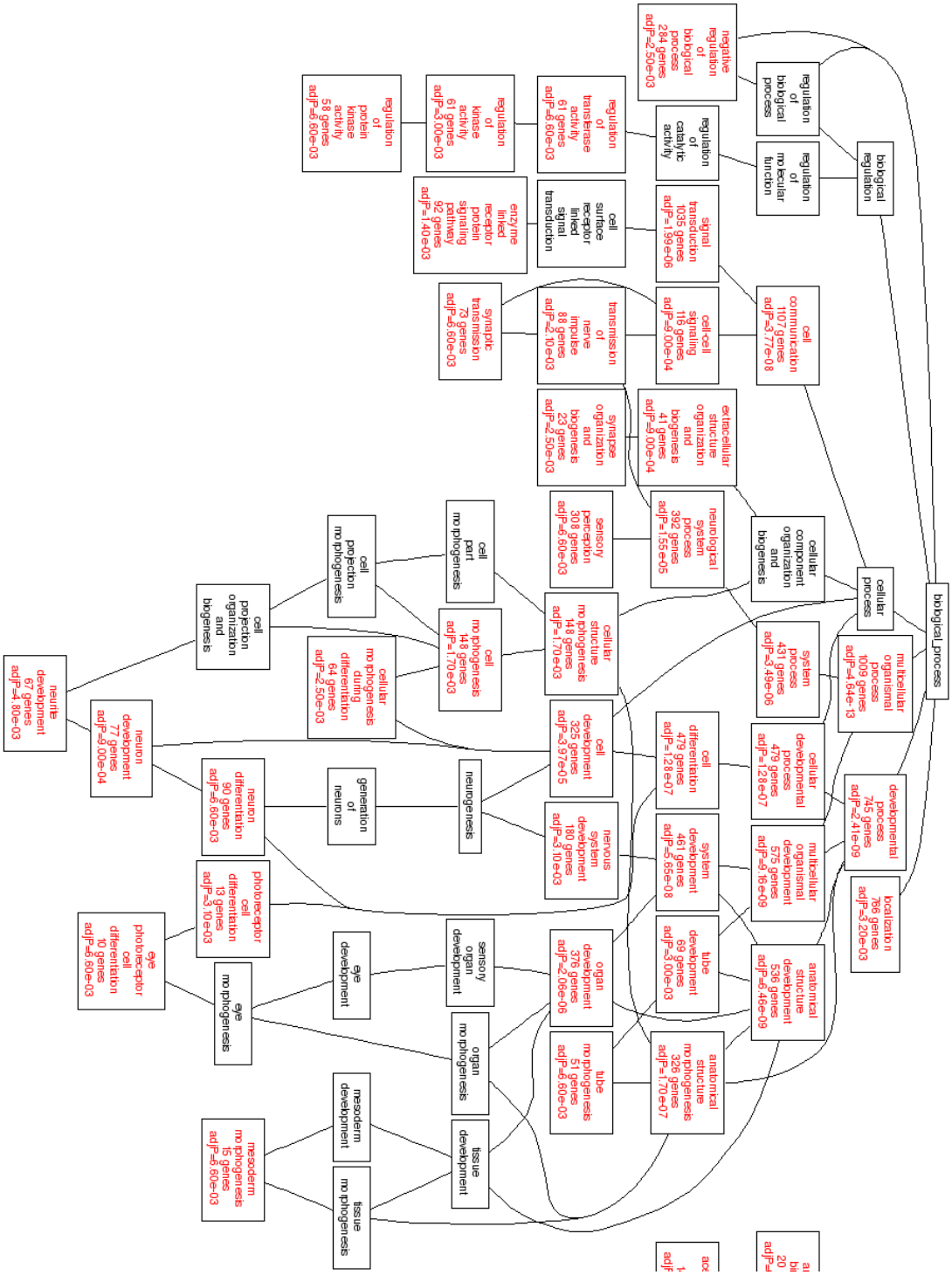
biological_process
cellular process
biological regulation
multicellular organismal process 1009 genes adjP=4.64e-13
developmental process 745 genes adjP=2.41e-09
localization 766 genes adjP=3.20e-03
cellular component organization and biogenesis
system process 431 genes adjP=3.49e-06
cellular developmental process 479 genes adjP=1.28e-07
multicellular organismal development 575 genes adjP=9.16e-09
anatomical structure development 536 genes adjP=6.46e-09
regulation of biological process
regulation of molecular function
negative regulation of biological process 284 genes adjP=2.50e-03
regulation of catalytic activity
cell communication 1107 genes adjP=3.77e-08
signal transduction 1035 genes adjP=1.99e-06
cell-cell signaling 116 genes adjP=9.00e-04
extracellular structure organization and biogenesis 41 genes adjP=9.00e-04
neurological system process 392 genes adjP=1.55e-05
sensory perception 308 genes adjP=6.60e-03
cell differentiation 479 genes adjP=1.28e-07
system development 461 genes adjP=5.65e-08
tube development 69 genes adjP=3.00e-03
anatomical structure morphogenesis 326 genes adjP=1.70e-07
regulation of transferase activity 61 genes adjP=6.60e-03
regulation of kinase activity 61 genes adjP=3.00e-03
regulation of protein kinase activity 58 genes adjP=6.60e-03
cell surface receptor linked signal transduction
enzyme linked receptor protein signaling pathway 92 genes adjP=1.40e-03
synaptic transmission 73 genes adjP=6.60e-03
transmission of nerve impulse 88 genes adjP=2.10e-03
synapse organization and biogenesis 23 genes adjP=2.50e-03
cell part morphogenesis
cell projection morphogenesis
cellular structure morphogenesis 148 genes adjP=1.70e-03
cell morphogenesis 148 genes adjP=1.70e-03
cellular morphogenesis during differentiation 64 genes adjP=2.50e-03
cell development 325 genes adjP=3.97e-05
nervous system development 160 genes adjP=3.10e-03
neurogenesis
generation of neurons
neuron differentiation 90 genes adjP=6.60e-03
cell projection organization and biogenesis
neurite development 67 genes adjP=4.80e-03
neuron development 77 genes adjP=9.00e-04
photoreceptor cell differentiation 13 genes adjP=3.10e-03
eye photoreceptor cell differentiation 10 genes adjP=6.60e-03
eye morphogenesis
eye development
sensory organ development
organ development 376 genes adjP=2.06e-06
organ morphogenesis
tube morphogenesis 51 genes adjP=6.60e-03
mesoderm development
tissue development
tissue morphogenesis
mesoderm morphogenesis 15 genes adjP=6.60e-03

c2)

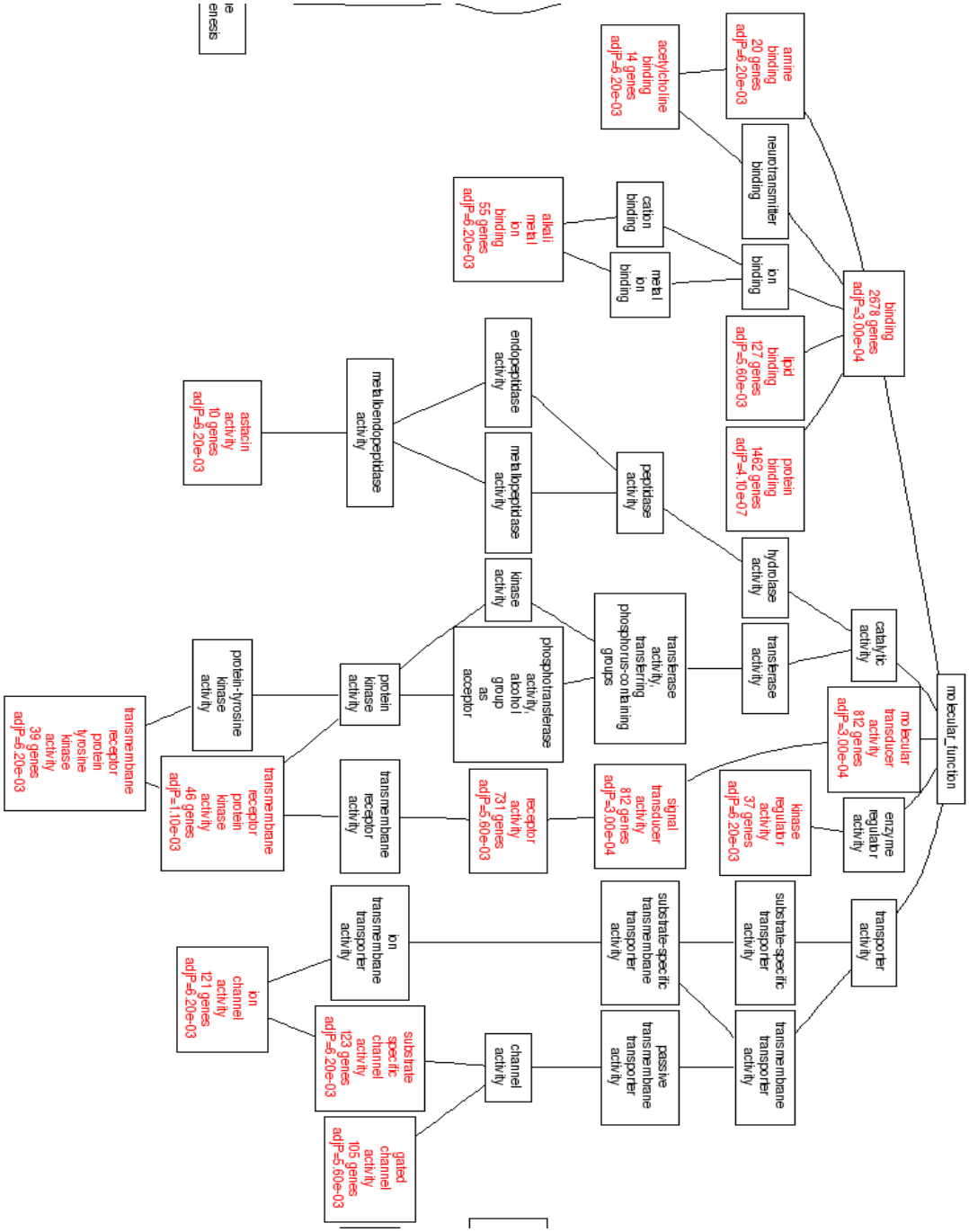
molecular_function
binding
2678 genes
adjP=3.00e-04
catalytic activity
transporter activity
enzyme regulator activity
molecular transducer activity
812 genes
adjP=3.00e-04
amine binding
20 genes
adjP=6.20e-03
acetylcholine binding
14 genes
adjP=6.20e-03
neurotransmitter binding
ion binding
lipid binding
127 genes
adjP=5.60e-03
protein binding
1482 genes
adjP=4.10e-07
alkali metal ion binding
55 genes
adjP=6.20e-03
cation binding
metal ion binding
hydrolase activity
peptidase activity
transferase activity
transferase activity, transferring phosphorus-containing groups
phosphotransferase activity, alcohol group as acceptor
endopeptidase activity
metalloendopeptidase activity
astacin activity
10 genes
adjP=6.20e-03
kinase activity
protein kinase activity
protein-tyrosine kinase activity
transmembrane receptor protein tyrosine kinase activity
39 genes
adjP=6.20e-03
transmembrane receptor protein kinase activity
46 genes
adjP=1.10e-03
signal transducer activity
812 genes
adjP=3.00e-04
receptor activity
731 genes
adjP=5.60e-03
transmembrane receptor activity
kinase regulator activity
37 genes
adjP=6.20e-03
substrate-specific transporter activity
substrate-specific transmembrane transporter activity
transmembrane transporter activity
passive transmembrane transporter activity
ion transmembrane transporter activity
channel activity
substrate specific channel activity
123 genes
adjP=6.20e-03
gated channel activity
105 genes
adjP=5.60e-03
ion channel activity
121 genes
adjP=6.20e-03

c3)

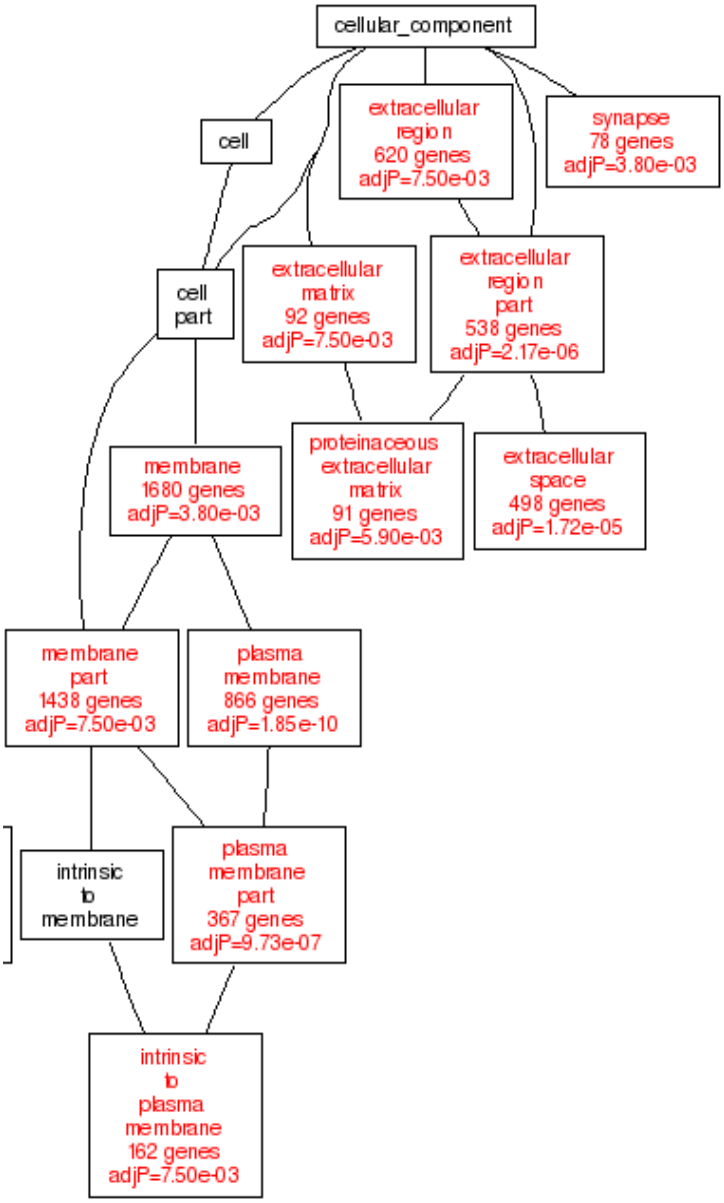
cellular_component
cell
extracellular region 620 genes adjP=7.50e-03
synapse 78 genes adjP=3.80e-03
cell part
extracellular matrix 92 genes adjP=7.50e-03
extracellular region part 538 genes adjP=2.17e-06
membrane 1680 genes adjP=3.80e-03
proteinaceous extracellular matrix 91 genes adjP=5.90e-03
extracellular space 498 genes adjP=1.72e-05
membrane part 1438 genes adjP=7.50e-03
plasma membrane 866 genes adjP=1.85e-10
intrinsic to membrane
plasma membrane part 367 genes adjP=9.73e-07
intrinsic to plasma membrane 162 genes adjP=7.50e-03

d)

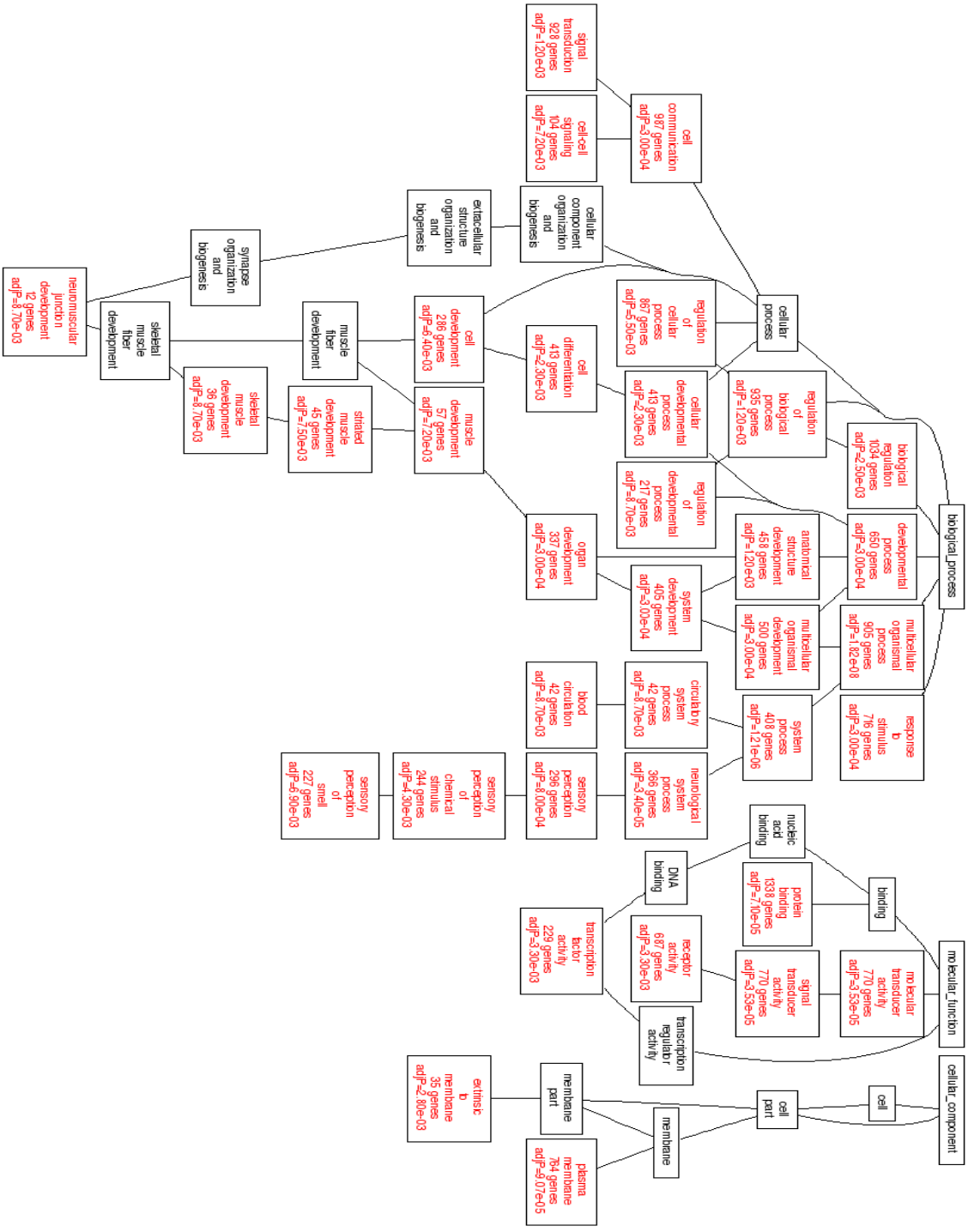
biological_process
cellular_component
molecular_function
cellular process
cell communication 987 genes adjP=3.00e-04
signal transduction 928 genes adjP=1.20e-03
cell-cell signaling 104 genes adjP=1.20e-03
cellular component organization and biogenesis
extracellular structure organization and biogenesis
synapse organization and biogenesis
neuromuscular junction development 12 genes adjP=8.70e-03
skeletal muscle fiber development
skeletal muscle development 36 genes adjP=8.70e-03
muscle fiber development
striated muscle development 45 genes adjP=1.50e-03
cell development 286 genes adjP=3.40e-03
muscle development 57 genes adjP=1.20e-03
regulation of cellular process 867 genes adjP=5.50e-03
cell differentiation 413 genes adjP=2.30e-03
cellular development process 413 genes adjP=2.30e-03
regulation of biological process 935 genes adjP=1.20e-03
regulation of development process 217 genes adjP=8.70e-03
organ development 337 genes adjP=3.00e-04
biological regulation 1034 genes adjP=2.50e-03
developmental process 650 genes adjP=3.00e-04
anatomical structure development 458 genes adjP=1.20e-03
system development 405 genes adjP=3.00e-04
multicellular organismal development 500 genes adjP=3.00e-04
multicellular organismal process 905 genes adjP=1.82e-08
response to stimulus 716 genes adjP=3.00e-04
circulatory system process 42 genes adjP=8.70e-03
blood circulation 42 genes adjP=8.70e-03
system process 408 genes adjP=1.21e-06
neurological system process 366 genes adjP=3.40e-05
sensory perception 296 genes adjP=6.00e-04
sensory perception of chemical stimulus 244 genes adjP=4.30e-03
sensory perception of smell 227 genes adjP=6.90e-03
nucleic acid binding
DNA binding
transcription factor activity 229 genes adjP=3.30e-03
protein binding 1338 genes adjP=7.10e-05
binding
receptor activity 687 genes adjP=3.30e-03
signal transducer activity 770 genes adjP=3.53e-05
molecular transducer activity 770 genes adjP=3.53e-05
transcription regulator activity
cell
cell part
membrane
membrane part
plasma membrane 764 genes adjP=9.07e-05
extrinsic to membrane 35 genes adjP=2.90e-03

e)

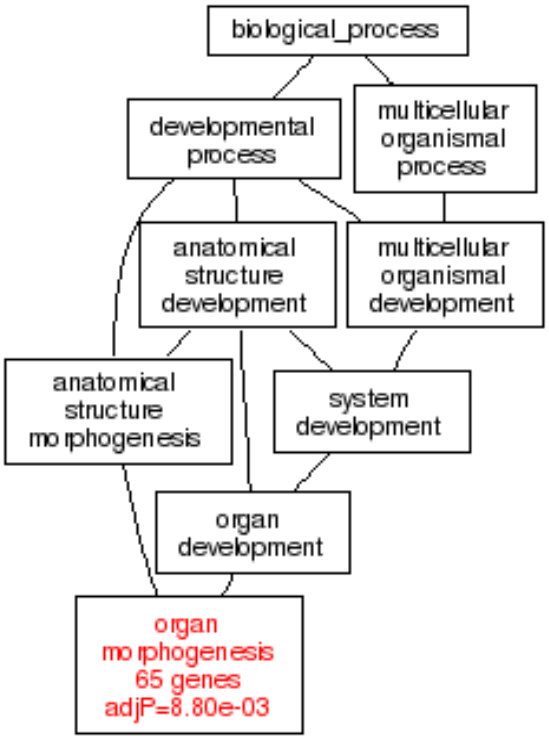
biological_process
developmental process
multicellular organismal process
anatomical structure development
multicellular organismal development
anatomical structure morphogenesis
system development
organ development
organ morphogenesis
65 genes
adjP=8.80e-03

f)

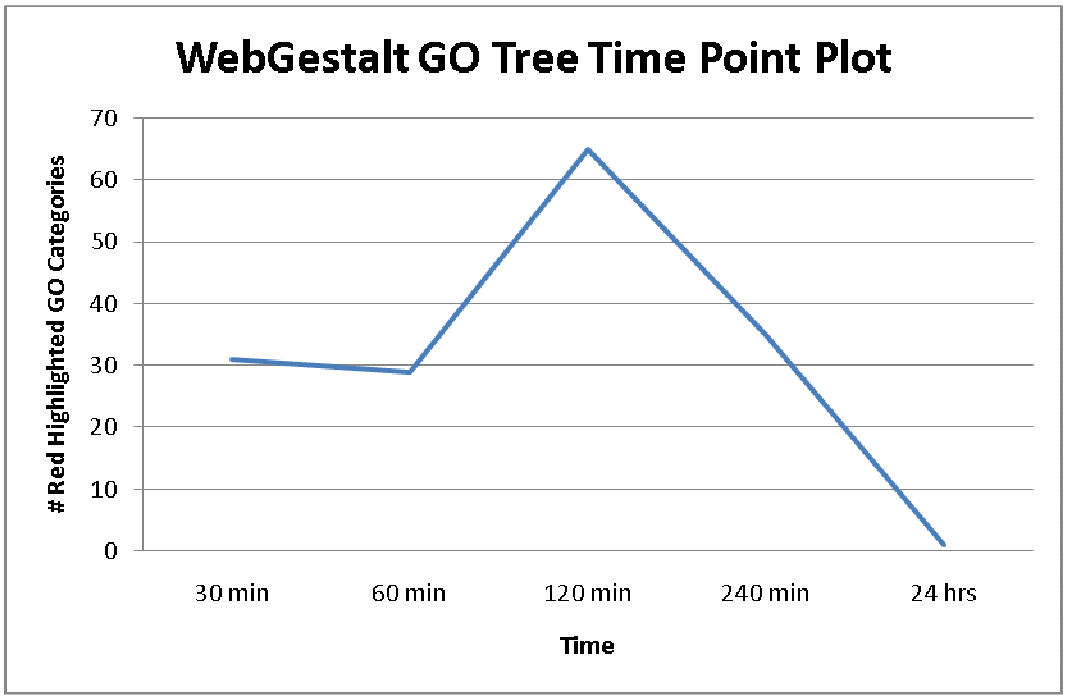

Figure 5: Web Gestalt GO trees of significantly overrepresented differentially expressed genes. Gene lists used has been treated with statistical threshold of 0.1 to -0.1 estimate and p-value < 0.15. Statistical settings used to generate GO trees include using Hypergeometric method, BH multiple test correction adjustment [20], significance level of 0.01 of adjusted p-value, and a gene category cutoff number of two. a) 30 minutes b) 60 minutes c1) 120 minutes "biological process" c2) 120 minutes "molecular function" c3) 120 minutes "cellular component" d) 240 minutes e) 24 hours f) Plot summary of the number of red highlighted GO categories versus time.

a)

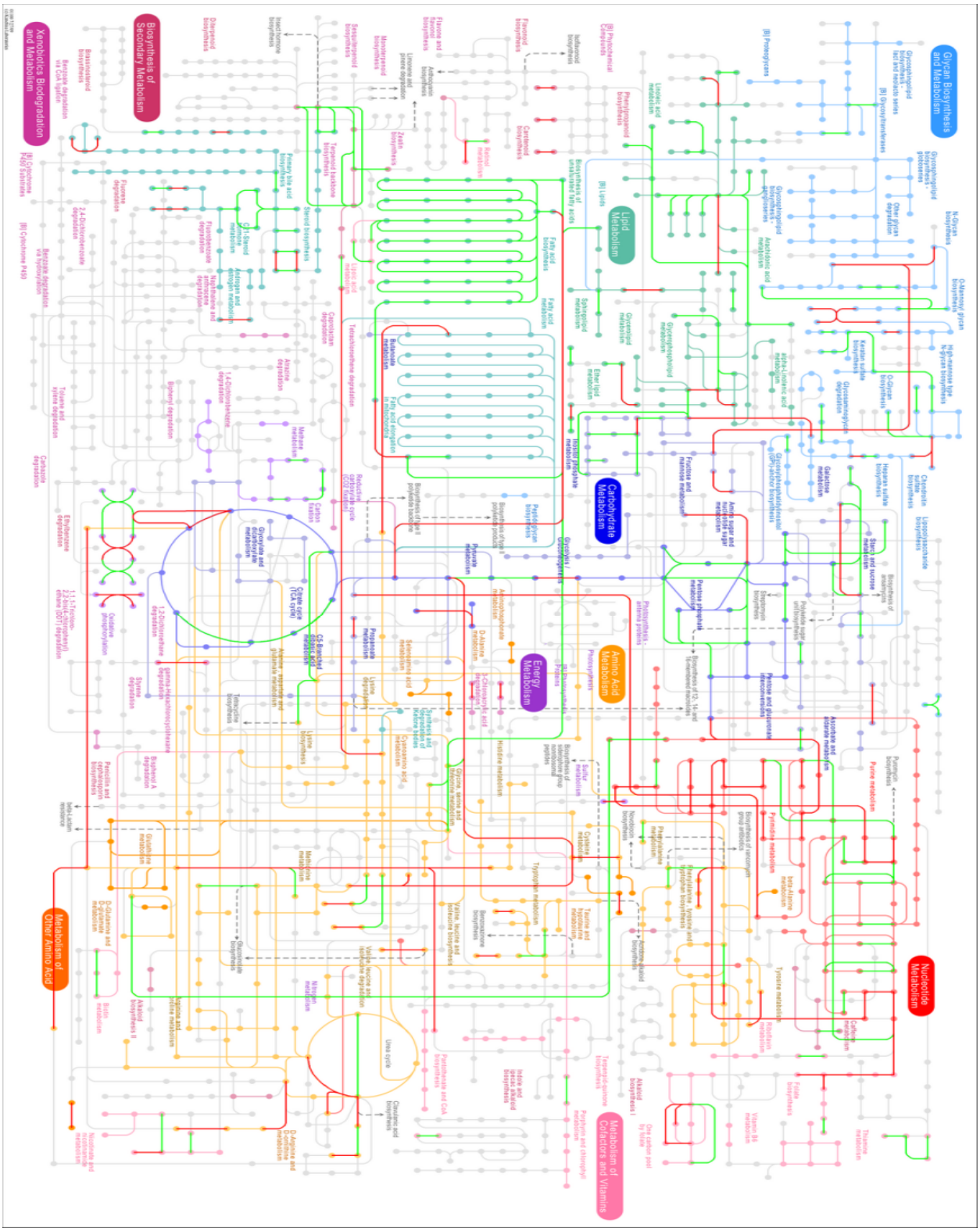
Glycan Biosynthesis and Metabolism
Lipid Metabolism
Carbohydrate Metabolism
Energy Metabolism
Amino Acid Metabolism
Nucleotide Metabolism
Metabolism of Cofactors and Vitamins
Metabolism of Other Amino Acid
Xenobiotics Biodegradation and Metabolism
Biosynthesis of Secondary Metabolism

b)

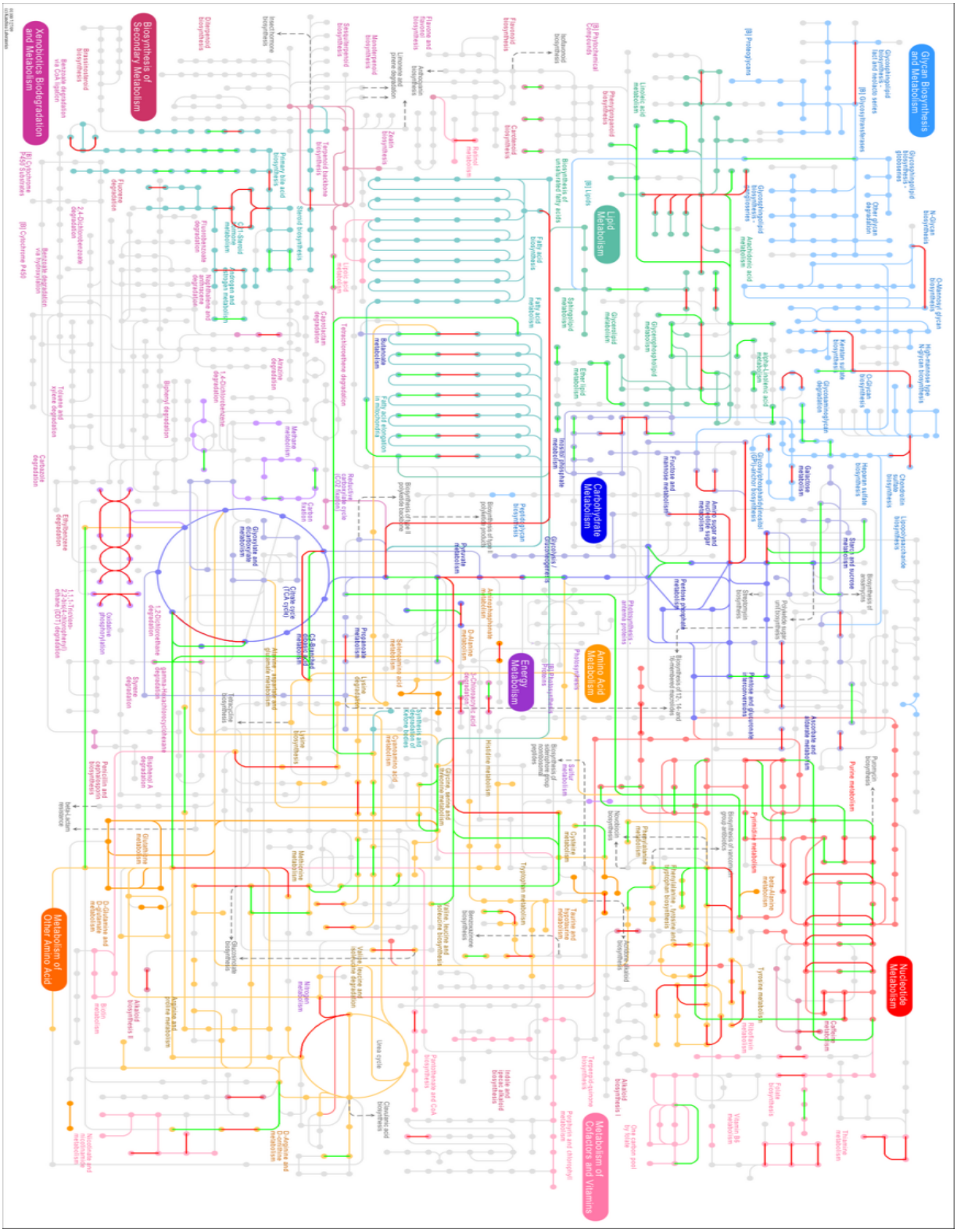
Glycan Biosynthesis and Metabolism
Lipid Metabolism
Carbohydrate Metabolism
Energy Metabolism
Amino Acid Metabolism
Nucleotide Metabolism
Metabolism of Cofactors and Vitamins
Metabolism of Other Amino Acid
Biosynthesis of Secondary Metabolism
Xenobiotics Biodegradation and Metabolism

c)

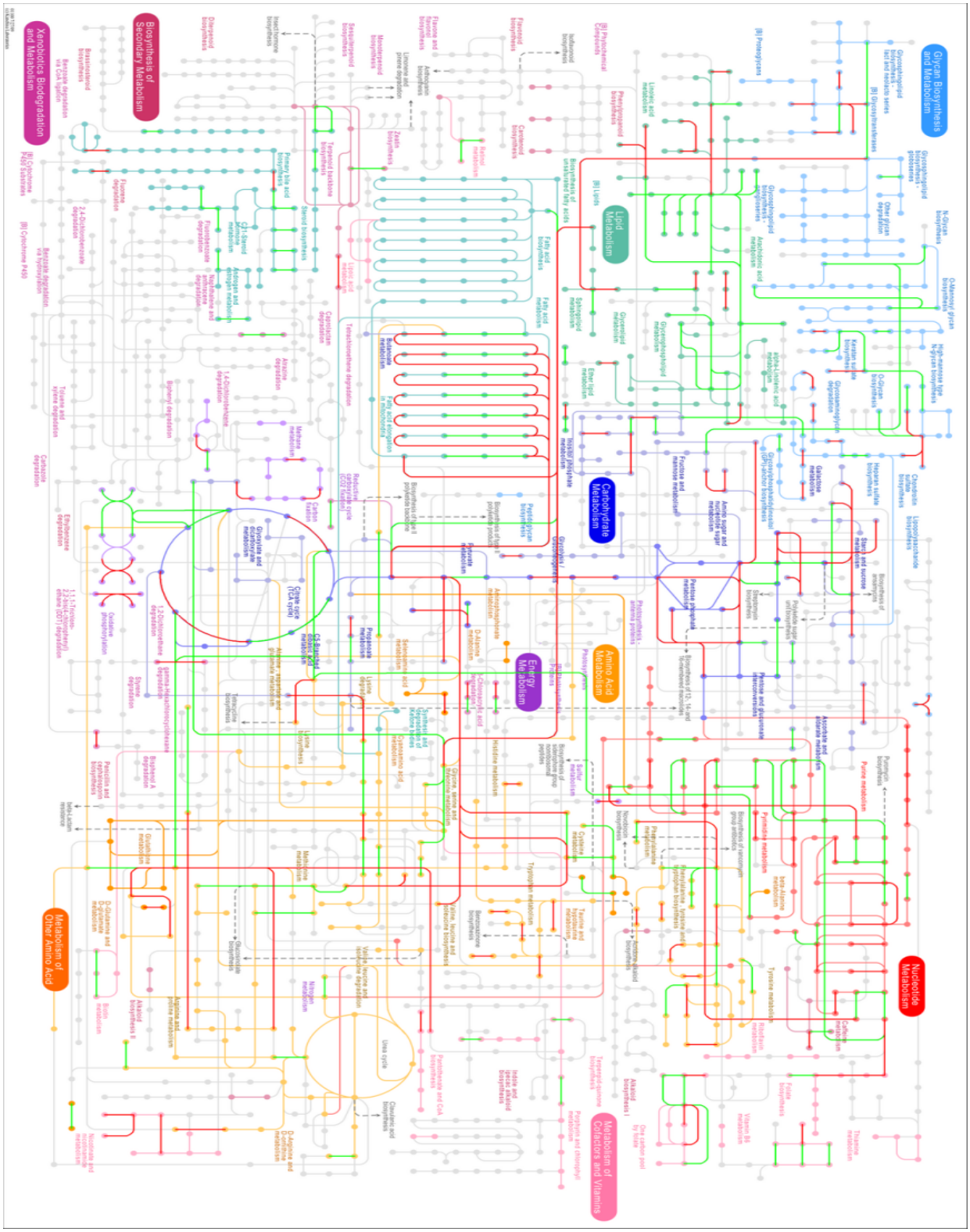
Glycan Biosynthesis and Metabolism
Lipid Metabolism
Carbohydrate Metabolism
Energy Metabolism
Amino Acid Metabolism
Nucleotide Metabolism
Metabolism of Cofactors and Vitamins
Metabolism of Other Amino Acid
Biosynthesis of Secondary Metabolism
Xenobiotics Biodegradation and Metabolism

d)

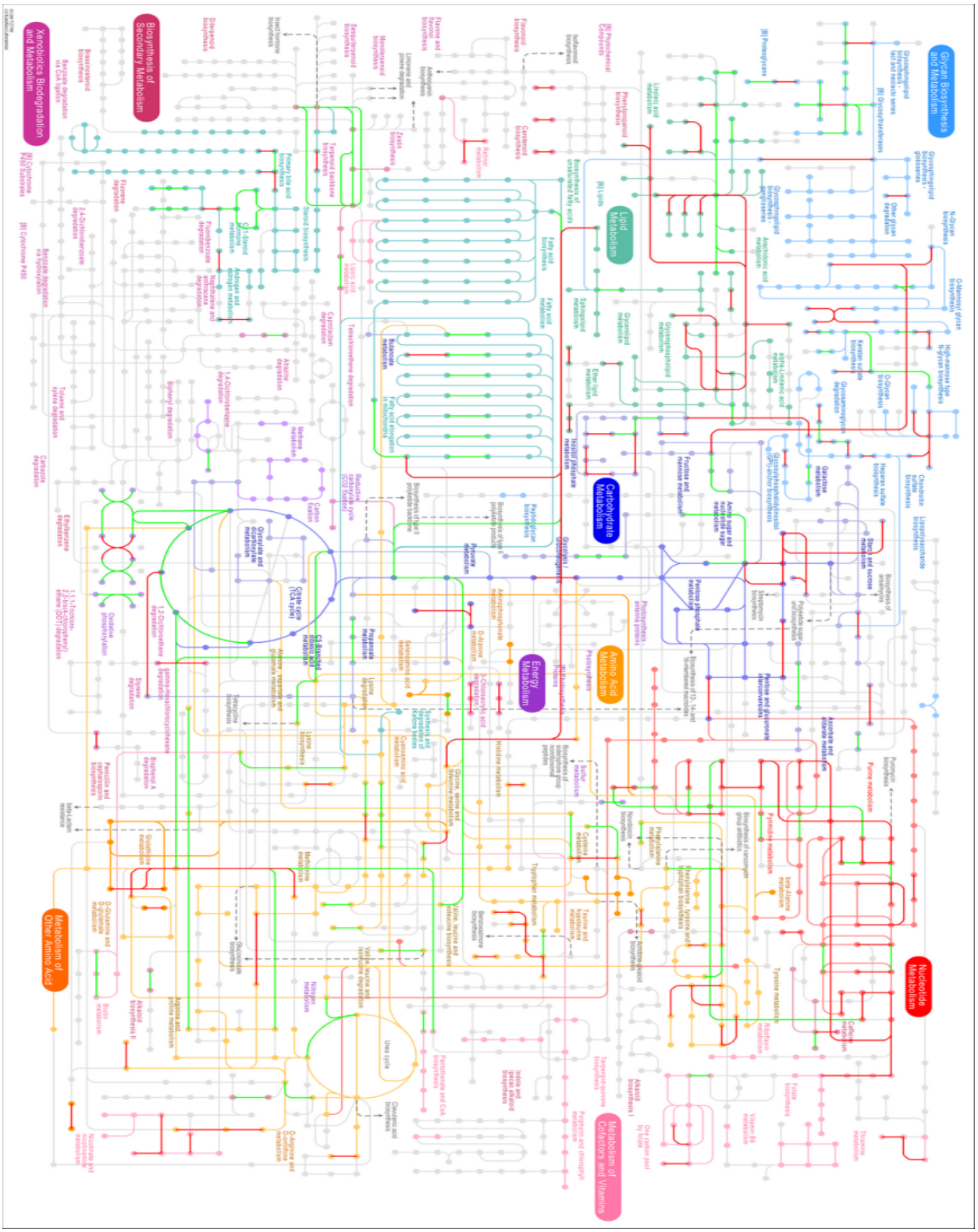
Glycan Biosynthesis and Metabolism
Lipid Metabolism
Carbohydrate Metabolism
Energy Metabolism
Amino Acid Metabolism
Nucleotide Metabolism
Metabolism of Cofactors and Vitamins
Metabolism of Other Amino Acid
Xenobiotics Biodegradation and Metabolism
Biosynthesis of Secondary Metabolism

e)

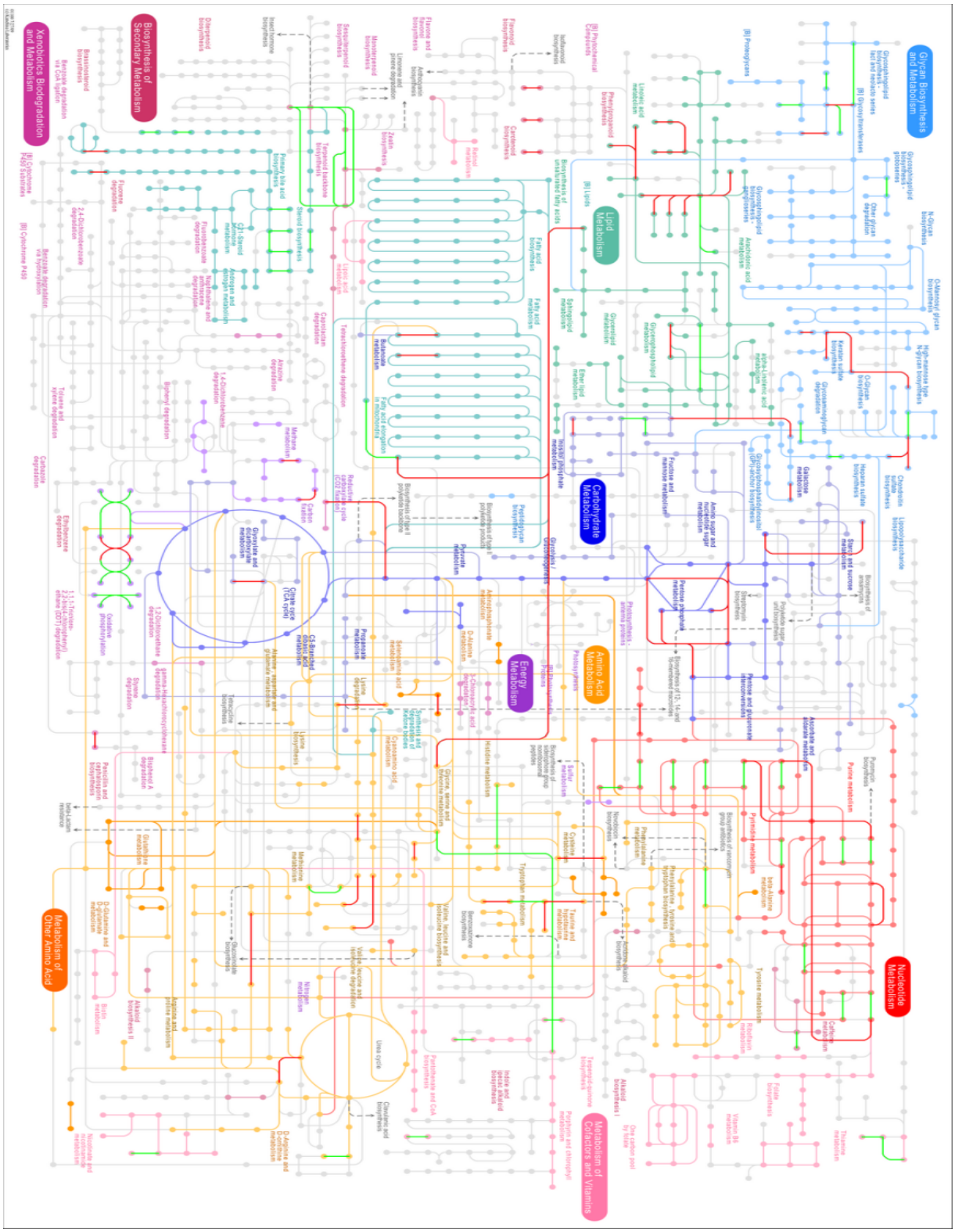
Glycan Biosynthesis and Metabolism
Lipid Metabolism
Carbohydrate Metabolism
Amino Acid Metabolism
Energy Metabolism
Nucleotide Metabolism
Metabolism of Cofactors and Vitamins
Metabolism of Other Amino Acid
Biosynthesis of Secondary Metabolism
Xenobiotics Biodegradation and Metabolism

Figure 6: These metabolic maps were generated from KEGG using a gene list generated from a statistical threshold of 0.1 to -0.1 estimate and p-value < 0.3. A bold red line indicates up-regulated differential expression and bold light green indicates down-regulated differential expression. a) 30 minutes b) 60 minutes c) 120 minutes d) 240 minutes e) 24 hours

Signal Transduction

As stated previously, the cell signaling in response to cell damage at the plasma membrane is not fully understood. GO categories falling under “response to stimulus” (Figure 5a) are significantly, differentially expressed at 30 minutes as detected by Web Gestalt. Among all differential gene lists studied, the most prominent group of differentially expressed genes pertained to G-protein coupled receptors labeled as olfactory receptors (Figure 7a). The majority of genes pertaining to this GO category are up-regulated. These receptors and resulting signal transduction could be playing a novel role as part of the recognition of plasma membrane disruption and corresponding response by the cell to the site of damage. Other mediating signal transducers were recorded (Figure 7b) but none differentially expressed as vast as G-protein coupled receptors.

a)

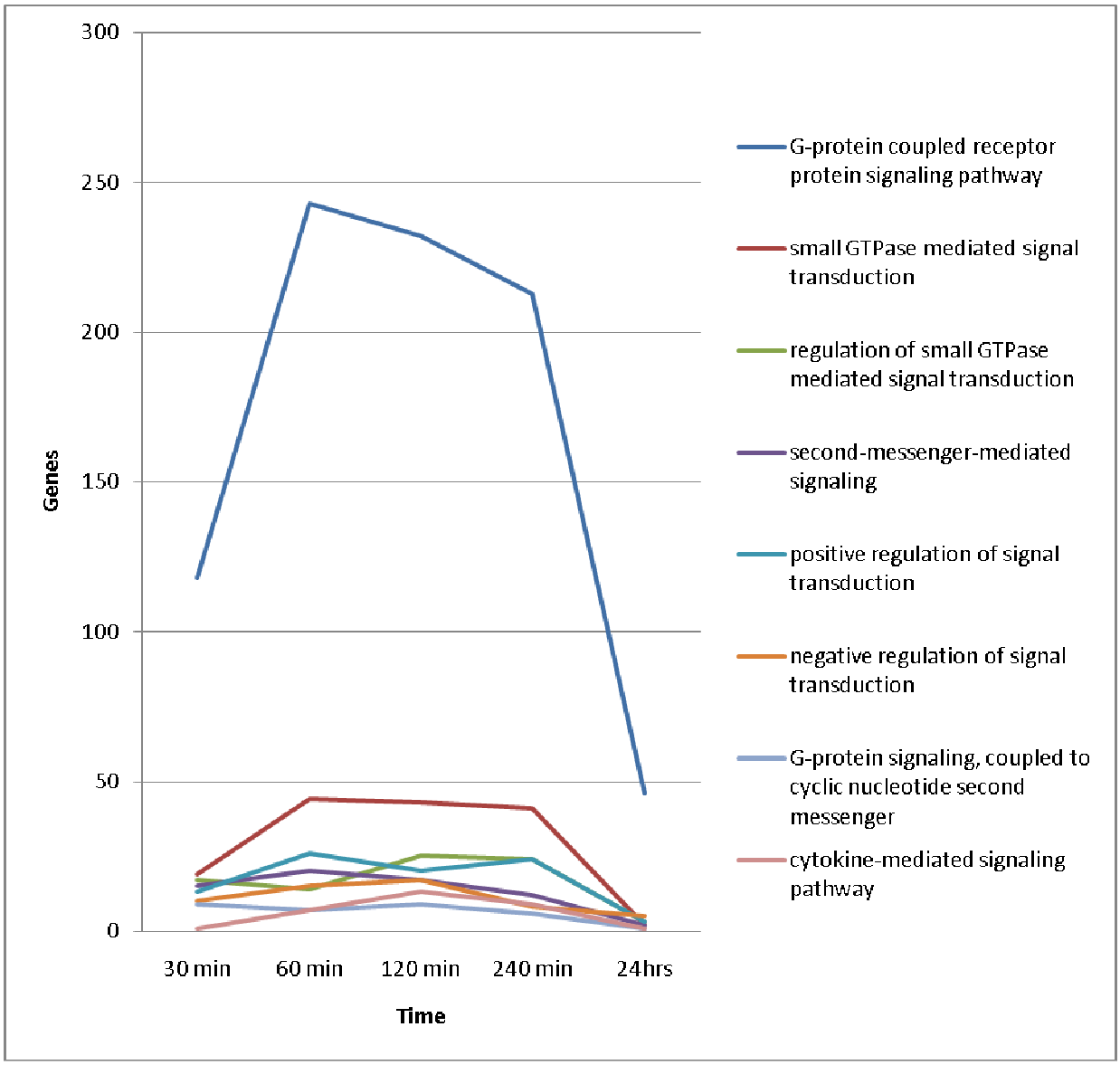
300
250
200
150
100
50
0
Genes
30 min
60 min
120 min
240 min
24hrs
Time
G-protein coupled receptor protein signaling pathway
small GTPase mediated signal transduction
regulation of small GTPase mediated signal transduction
second-messenger-mediated signaling
positive regulation of signal transduction
negative regulation of signal transduction
G-protein signaling, coupled to cyclic nucleotide second messenger
cytokine-mediated signaling pathway

b)

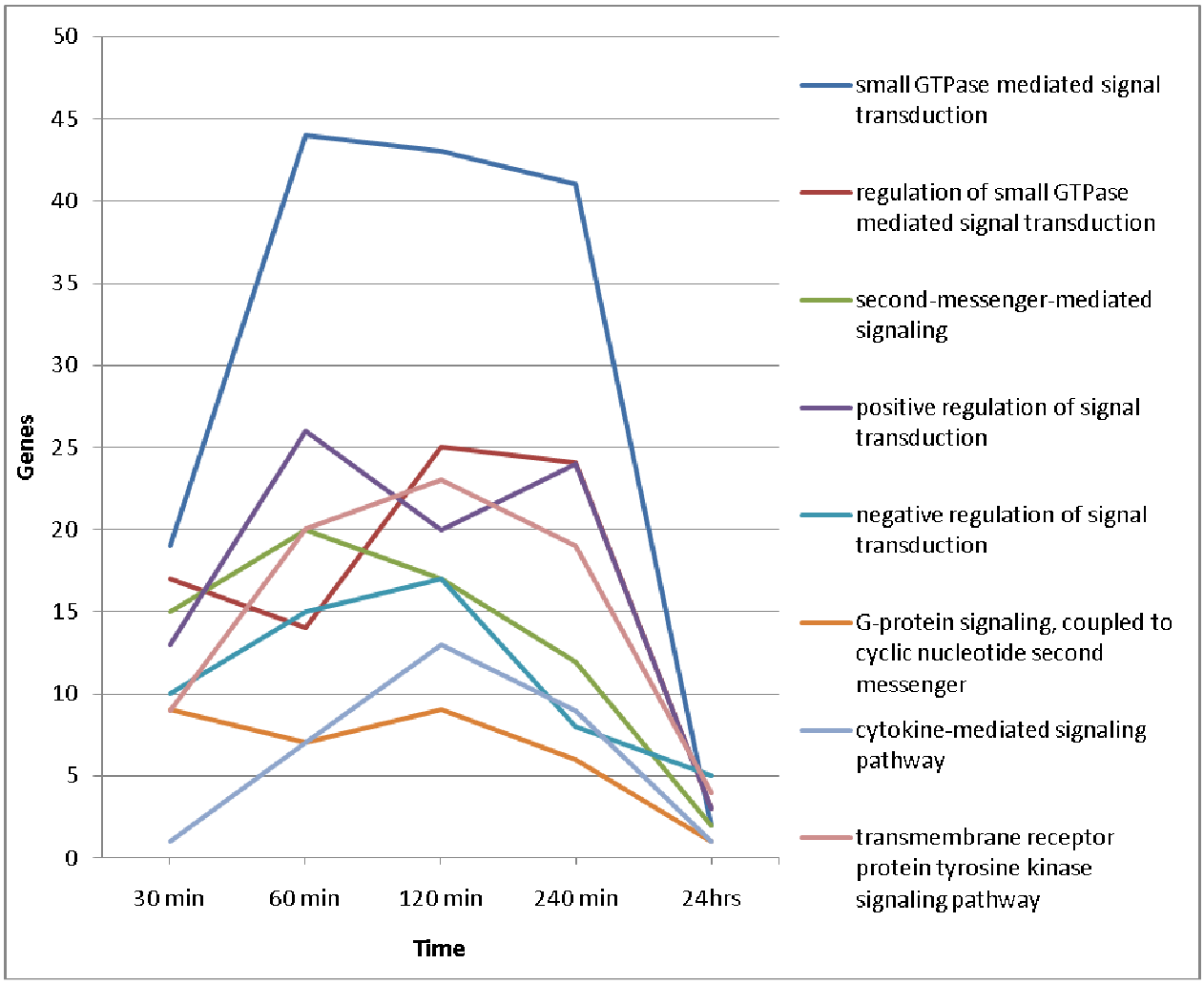

Figure 7: Plot of GO terms relating to signal transduction. Gene list used to generate plot has been treated with statistical threshold of 0.1 to -0.1 estimate and p-value < 0.15. a) Plot focus on "G-protein coupled receptor protein signaling pathway". Majority of genes pertaining to this GO category were up-regulated. b) Blow-up of other relating GO terms minus "G-protein coupled receptor protein signaling pathway"

Re-establishment of Homeostasis

With the impalement of the cell, ion homeostasis would be expected to be disturbed. An example would be the influx of calcium expected or loss of intracellular ions. Evidence supporting the re-establishment of homeostatasis within the cell following impalement is shown in Figure 8.

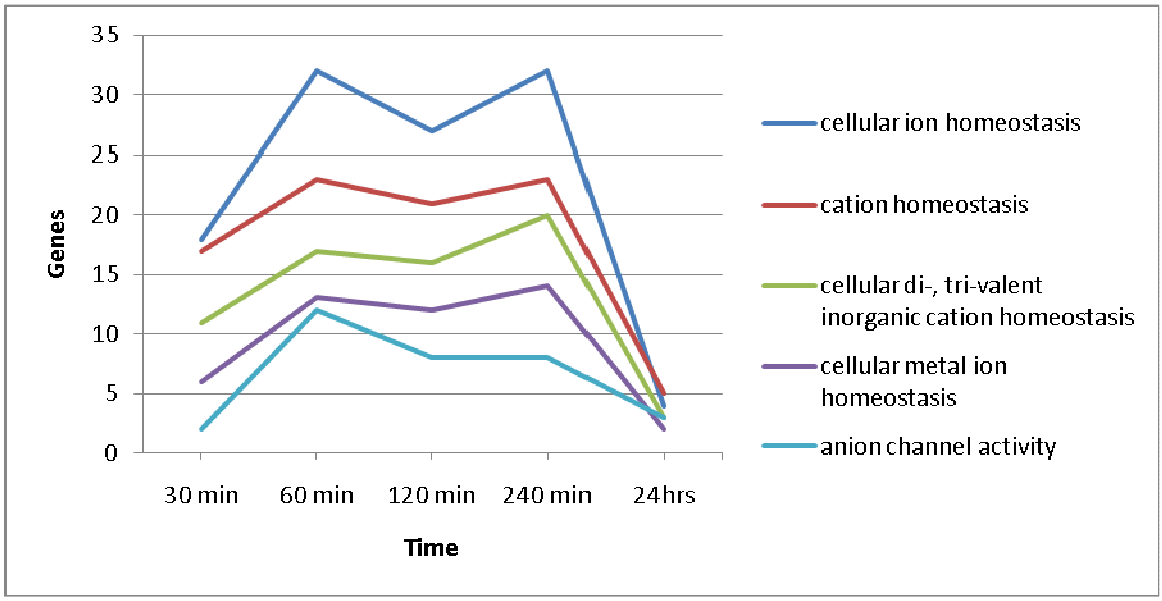

Figure 8: Plot of GO terms corresponding to ion channel activity. Genes in these GO categories are a mix of being up-regulated and down-regulated throughout out the time course. Gene list used to generate plot has been treated with statistical threshold of 0.2 to -0.2 estimate and p-value < 0.15.

Plasma Membrane Repair

The resealing of the plasma membrane must take place almost immediately to prevent the cell from lysing. The earliest experimental time point used was 30 minutes but we still see evidence coinciding with previously stated literature. Expected significantly, differentially expressed genes identified by Web Gestalt (Figure 5) are predominantly located at the plasma membrane up to 240 minutes. The GO term "lysosome" is differentially represented and diminishes by 24 hours (Figure 9). In addition, cytoskeleton related differential expression was evident (Figure 10) with a focus on gene ontology relating to actin and microtubules which is consistent with previous stated literature [9]. Further evidence may be derived from KEGG metabolic maps showing activity pertaining to lipid metabolism and disappears by 24 hours. Finally, proteolysis activity (Figure 11) would indicate repair of damaged proteins by 24 hours.

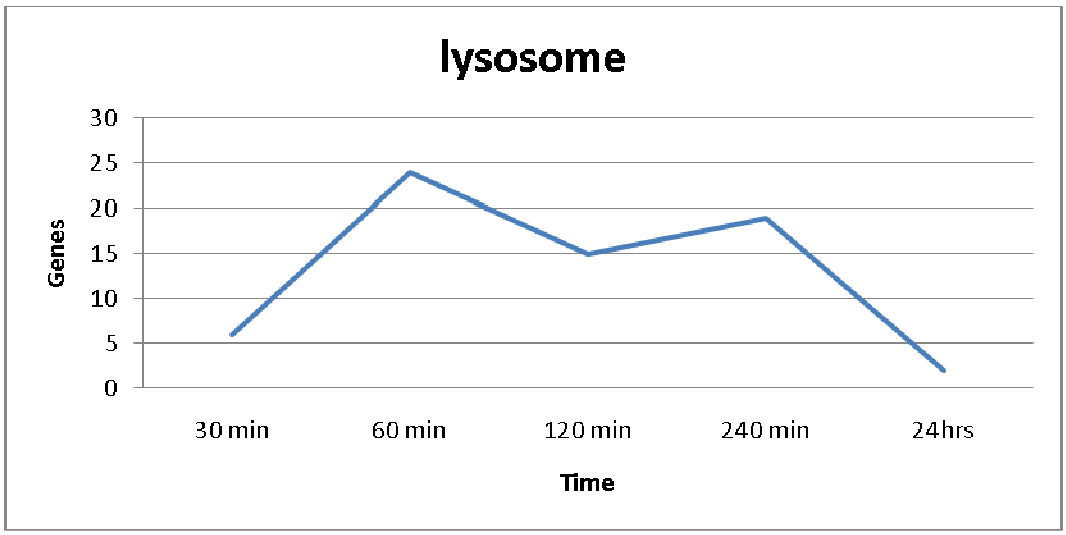

Figure 9: Plot of GO term "Lysosome". Majority of genes are up-regulated throughout the time course. Gene list used to generate plot has been treated with statistical threshold of 0.2 to -0.2 estimate and p-value < 0.15.

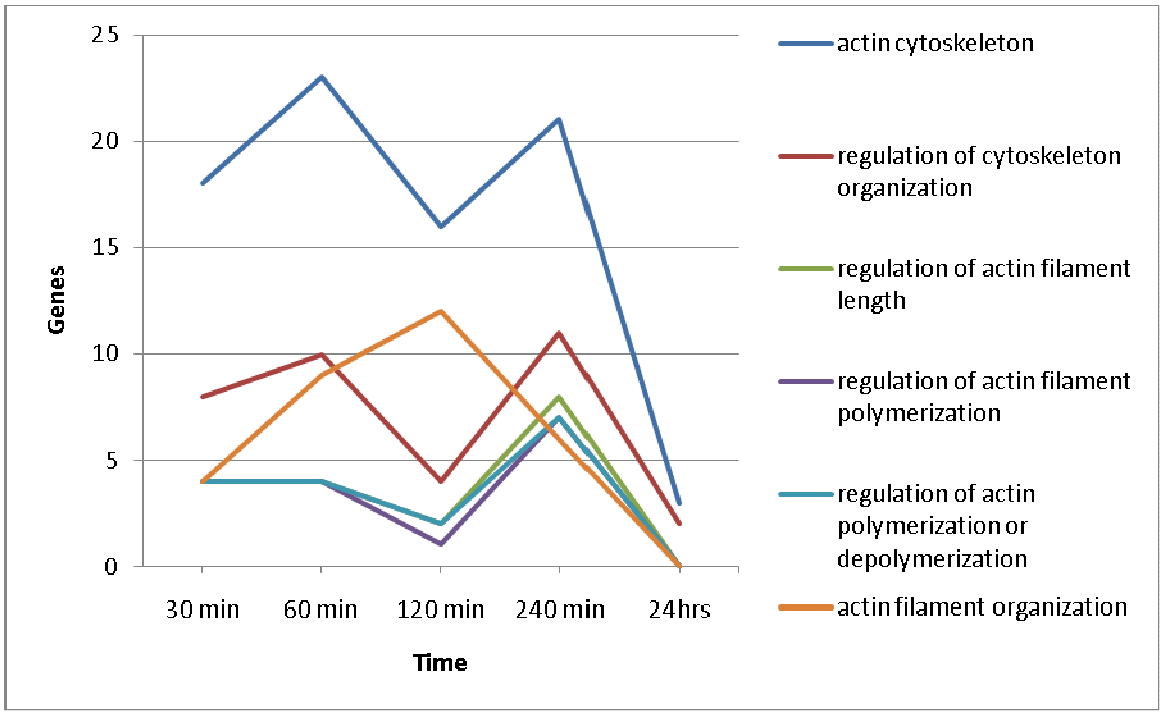

Figure 10: Plot of GO terms pertaining to activity at the cytoskeleton. Genes pertaining to these GO categories are not uniformly up or down regulated. Gene list used to generate plot has been treated with statistical threshold of 0.2 to -0.2 estimate and p-value < 0.15.

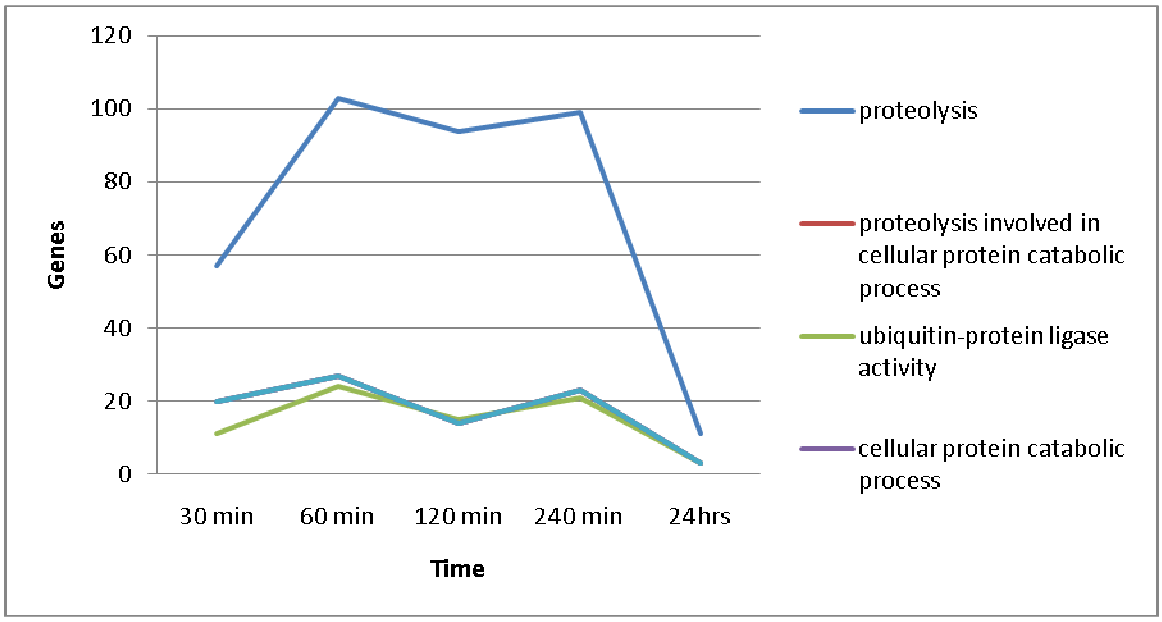

Figure 11: Plot of GO terms pertaining to protein degradation. Majority of genes in these GO categories are down-regulated between 30 to 60 minutes and become up regulated by 240 minutes. Gene list used to generate plot has been treated with statistical threshold of 0.2 to -0.2 estimate and p-value < 0.15.

Extracellular Matrix

In addition to over-representation of plasma membrane genes in the differentially-expressed gene sets, the genes involved in extracellular regions are highly active by 120 minutes. Genesis GO pies indicate overrepresentation of the “proteinaceous extracellular matrix” (Figure 12). Also, the continuous differential expression surrounding glycan metabolism (Figure 6) throughout the time course has provided candidates for a potential sealing action around the resident nanofiber during and after cell membrane repair. Upon further analysis one specific candidate for further testing; heparan sulfate; was identified by KEGG pathway maps (Figure 13)

that show consistent up regulation of heparan sulfate biosynthesis. An antibody test against heparan sulfate would confirm the role these glycans play.

a)

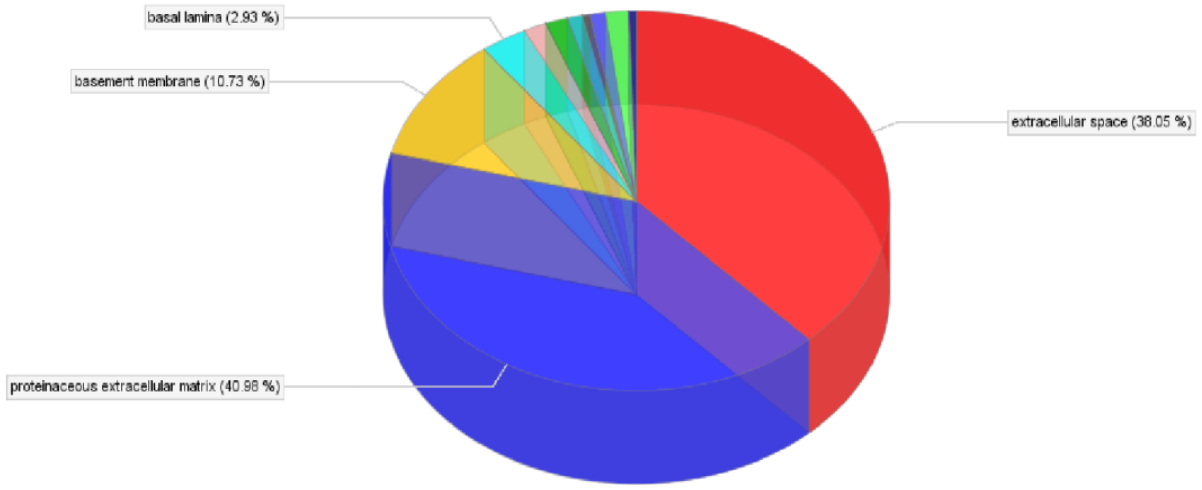

b)

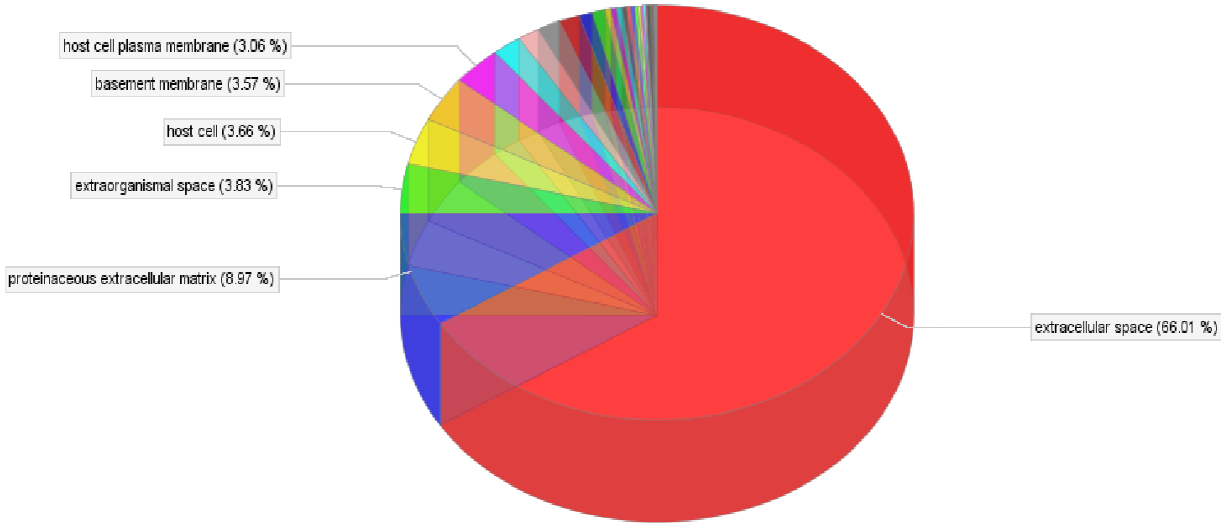

Figure 12: Genesis GO pies for the GO term “extracellular region part” at 120 minutes. Gene list used to generate plot has been treated with statistical threshold of 0.1 to -0.1 estimate and p-value

< 0.3. a) GO pie of gene list with 361 GO relations and 159 genes belonging to this category b) Complete chart of GO terms for “extracellular region part”

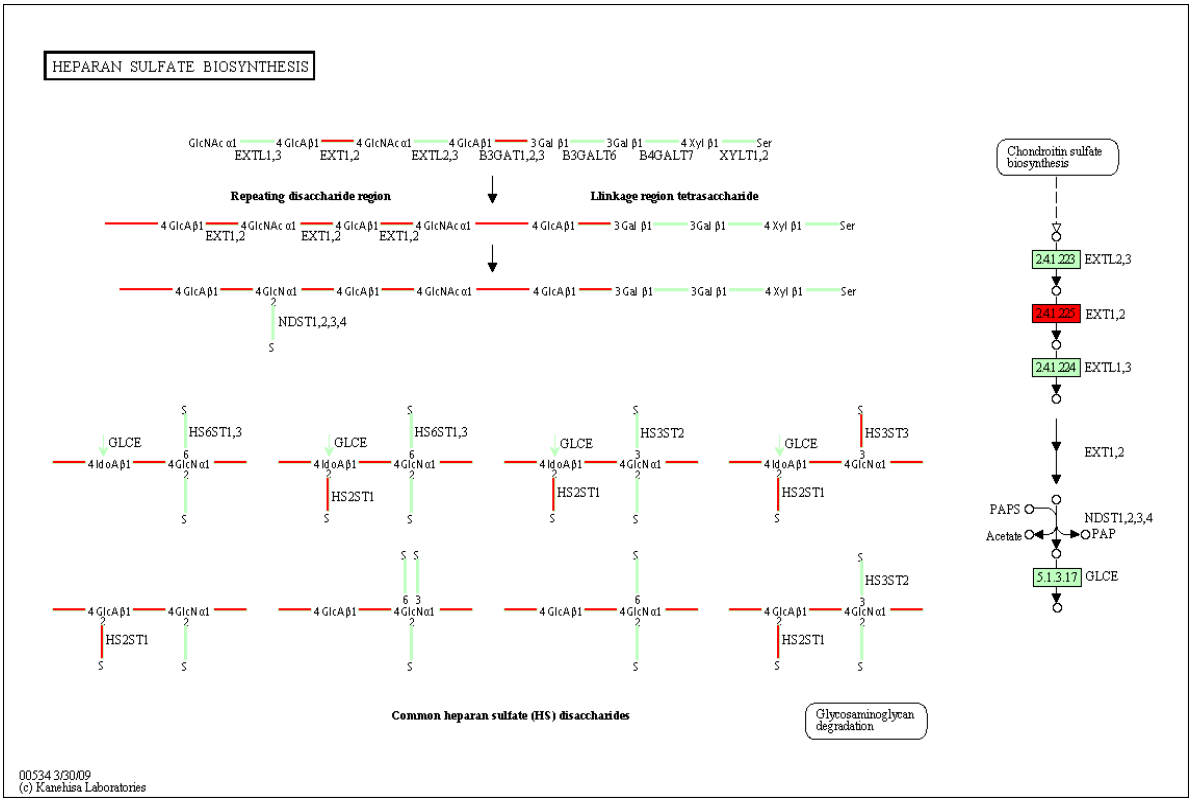

Figure 13: KEGG pathway map of Heparan Sulfate Biosynthesis at 120 minutes. Red fill indicates up-regulation, dark green fill indicates down-regulation, and light green indicates gene was found in the KEGG database but is neither up nor down regulated. Grey bars indicate genes are not known or not found in the KEGG database. Gene list used to generate pathway map has been treated with statistical threshold of 0.1 to -0.1 estimate and p-value < 0.3

Nucleus

Web Gestalt identified significant number of differentially expressed genes at the nucleus at 30 minutes (Figure 5a). Illustration of GO categories pertaining to nucleus overrepresentation is shown in Figure 15a (observed) versus Figure 15b (complete GO). This observation is consistent with the previous statement on the success of transfection or "impalefection" of CHO cells with GFP plasmid as the penetration of the nucleus is necessary. Furthermore, analysis of the impact of any DNA damage (Figure 14) led to no significant detection with respect to Web Gestalt and GO categories reported indicate no leading to a terminal response such as apoptosis.

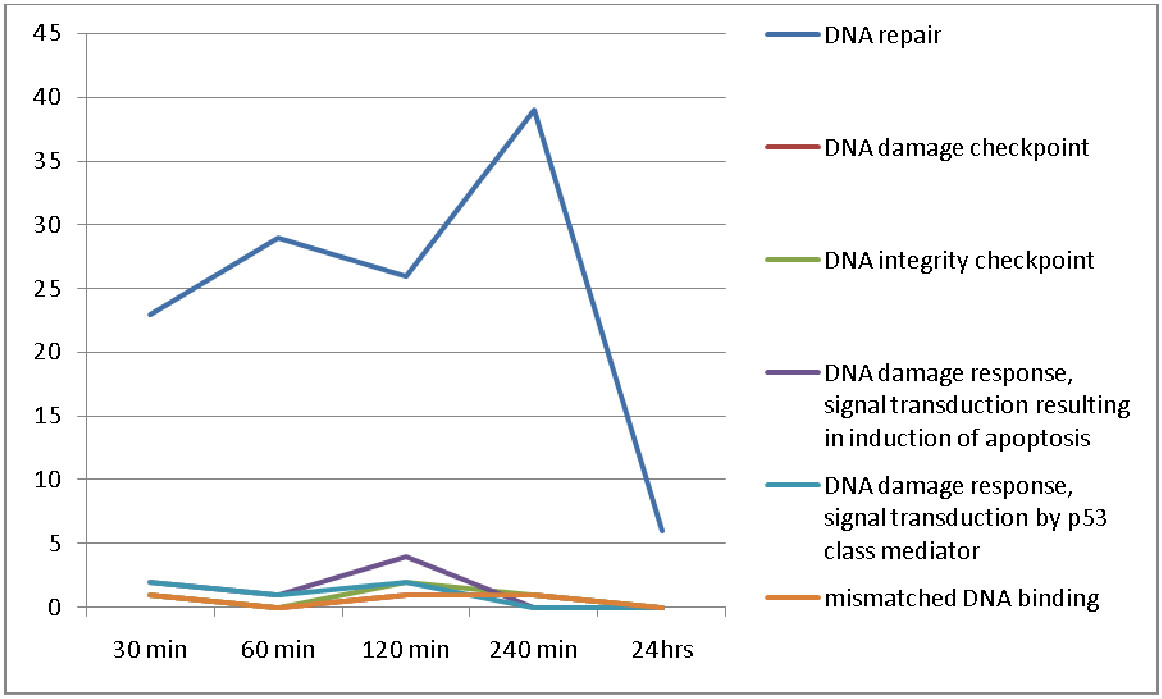

Figure 14: Plot of GO terms relating damage to DNA. Gene list used to generate plot has been treated with statistical threshold of 0.2 to -0.2 estimate and p-value < 0.15.

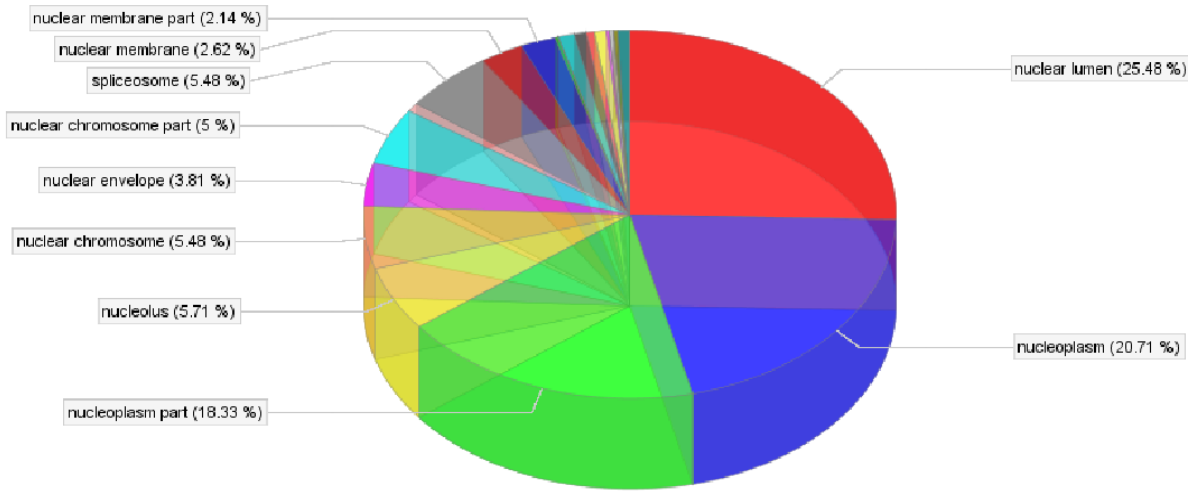

a)

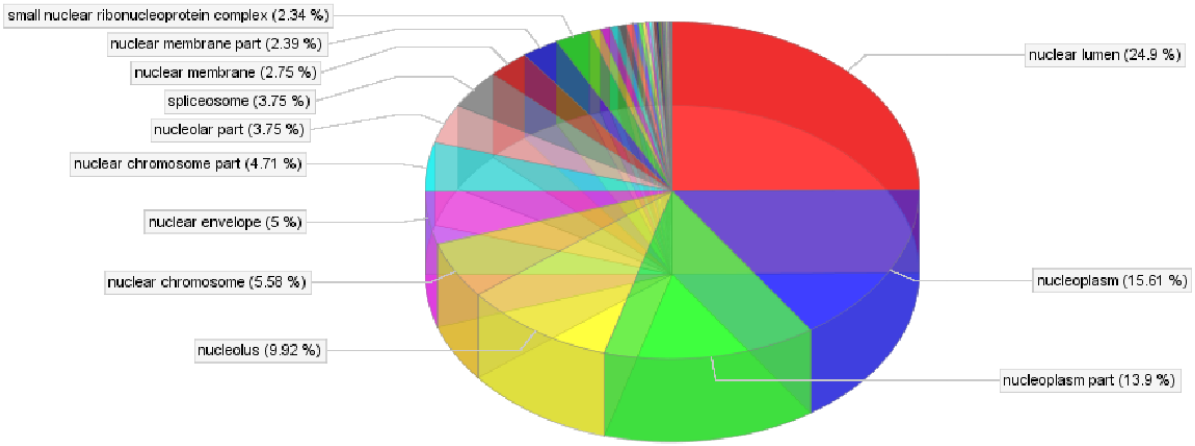

b)

Figure 15: Genesis GO pies for the GO term “nuclear part.” Gene list used to generate plot has been treated with statistical threshold of 0.1 to -0.1 estimate and p-value < 0.3. a) GO pie of gene list with 876 GO relations and 166 genes belonging to this category b) Complete GO of “nuclear part”

Apoptosis

Because of the inherent chaos caused by cell impalement and influx of calcium, one of the most surprising results was the lack of induction of apoptosis (Figure 16). Web Gestalt did not identify significant differential expression of GO categories belonging to apoptosis (Figure 5) and pathway analysis by KEGG (Figure 17) indicates no induction via p53 or other major regulators. In fact, pathway analysis suggests a regulation of apoptosis driving toward cell survival.

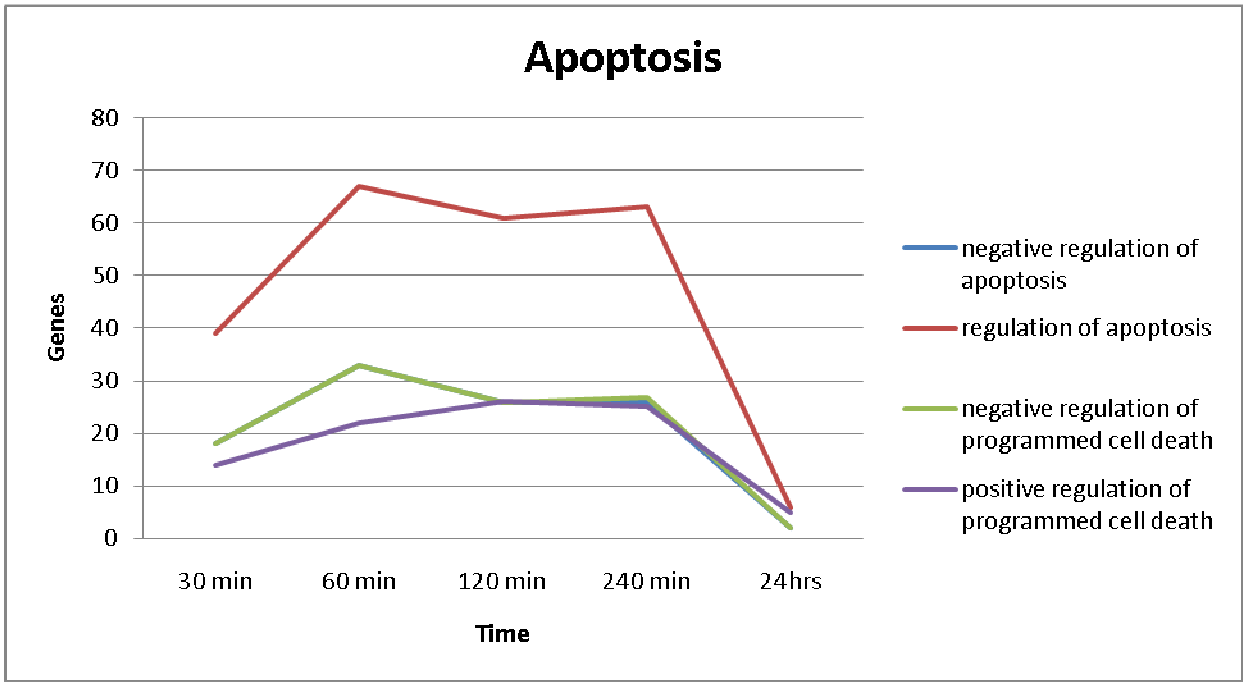

Figure 16: Plot of GO terms pertaining to apoptosis. Gene list used to generate plot has been treated with statistical threshold of 0.2 to -0.2 estimate and p-value < 0.15.

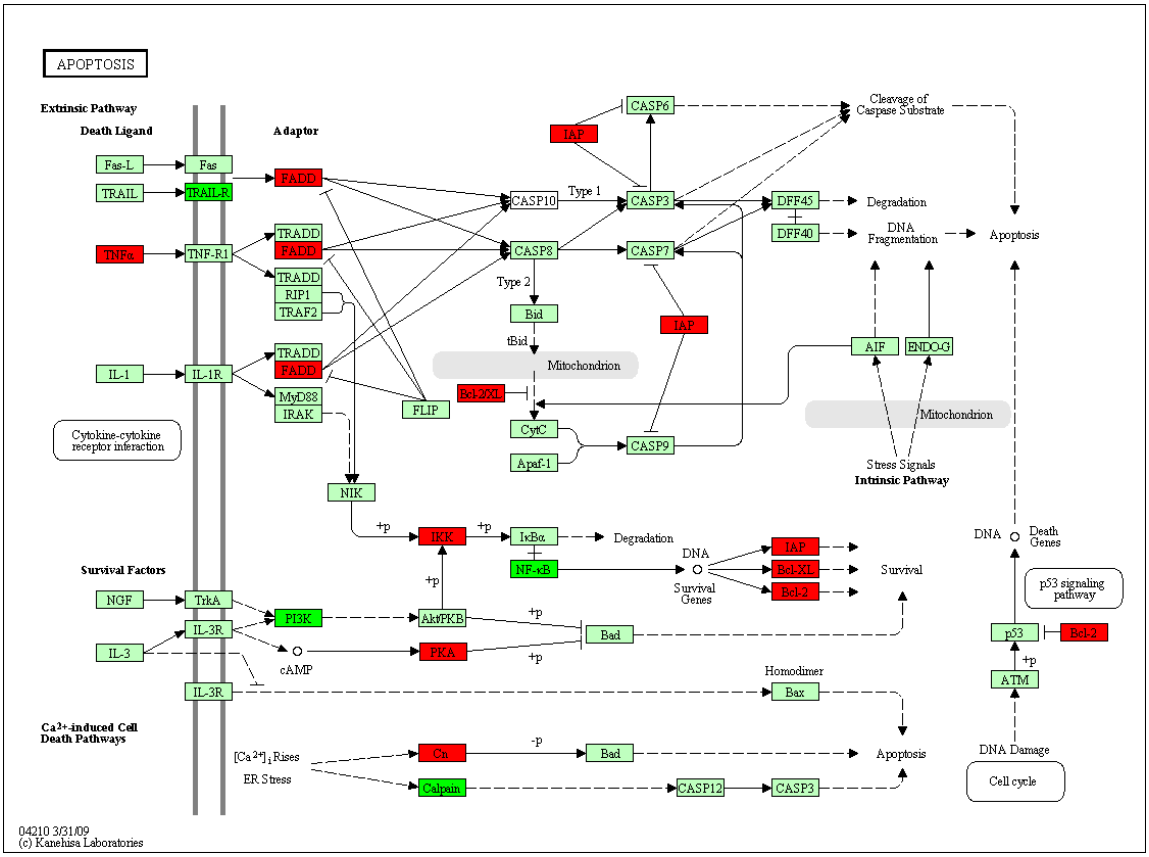

Figure 17: KEGG pathway map for Apoptosis at 60 minutes. Red fill indicates up-regulation, dark green fill indicates down-regulation, and light green indicates gene was found in the KEGG database but is neither up nor down regulated. Grey bars indicate genes are not known or not found in the KEGG database. Gene list used to generate pathway map has been treated with statistical threshold of 0.1 to -0.1 estimate and p-value < 0.3

CHAPTER IV

CONCLUSION

Cellular impalement and impalefection of cells on nanofibers is a new method of introducing genes into cells, and may have a role in regulating gene expression when used as a coating for clinical implants. To determine if impalefection resulted in transient or permanent cell metabolic disruption, we used microarrays to identify the changes in gene expression at multiple time points up to 24 hours following impalement. The most significant purpose of this study was to demonstrate that by 24 hours post-impalement, the impaled cells have resumed a near normal gene expression pattern. This suggests that the cells have adapted to the resident nanofiber, and are in the returning to normal metabolism. This observation is by itself remarkable, considering the initial chaotic gene expression response, and the presence of a foreign object permanently penetrating both the plasma and nuclear membranes. Considering the near normal gene expression it is reasonable to conclude that additional perturbations of the transcriptome by transgenes or miRNA can be discriminated at the transcriptional level.

In addition to this accomplishment, we have identified similarities and potentially novel responses related to membrane repair. However, cell impalement is considerably different from previous membrane repair studies and further work needs to be done. As

such, these studies provide a wealth of testable hypotheses about membrane repair, cell wounding responses, and novel mechanisms related to resident nanoparticles. For example, the role of glycans, specifically heparan sulfate, as potential sealing factor at the plasma membrane could be tested with existing heparan sulfate antibodies. Also, the role of G-protein receptors (identified largely as olfactory receptors) as part of the signaling pathway in response to impalement needs to be better understood. The use of siRNA knockdowns of specific receptors, or families of receptors, could provide important information about the cellular response to nanoparticle insults. One of the most surprising findings in this study was the lack of apoptosis induction. Although lack of apoptosis may go against intuition, it is possible that the artificial conditions of nanofiber impalement are not recognized by the cell, and thus has no programmed response. It will be interesting to test whether these cells are strongly resistant to inducers of apoptosis, or whether they are relatively fragile and easily pushed into apoptosis. Finally, because the cell has recovered from impalement by 24 hours, it will be possible to test an abundance of responses to *neighboring* (non-impaled) cells when impaled cells are producing transgenes. For example, in stem-cells, secreted factors that regulated determination events may be identified and perhaps even quantitated using index nanofiber cell-arrays. The use of nanofibers as a cell-regulatory coating for bioimplants could provide previously unobtainable control of neighboring cell responses to biological implants used to regulated disease.

REFERENCES

1. Doherty, K. R., McNally, E. M. Repairing the tears: dysferlin in muscle membrane repair. Trends Mol. Med. 9, 327–330 (2003).
2. Bansal, D., Campbell, K. P. Dysferlin and the plasma membrane repair in muscular dystrophy. Trends Cell Biol. 14, 206–213 (2004).
3. Bazan, N. G., Marcheselli, V. L. & Cole-Edwards, K. Brain response to injury and neurodegeneration: endogenous neuroprotective signaling. Ann. NY Acad. Sci. 1053,137–147 (2005).
4. McNeil, P. L., Kirchhausen, T. An emergency response team for membrane repair. Nature Rev. Mol. Cell Biol. 6, 499–505 (2005).
5. Steinhardt, R. A., Bi, G., Alderton, J. M. Cell membrane resealing by a vesicular mechanism similar to neurotransmitter release. Science 263, 390–393 (1994).
6. Miyake, K., McNeil, P. L. Vesicle accumulation and exocytosis at sites of plasma membrane disruption. J. Cell Biol. 131, 1737–1745 (1995).
7. Terasaki, M., Miyake, K., McNeil, P. L. Large plasma membrane disruptions are rapidly resealed by Calcium-dependent vesicle-vesicle fusion events. J. Cell Biol. 139, 63–74 (1997).
8. McNeil, P. L., Vogel, S. S., Miyake, K., Terasaki, M. Patching plasma membrane disruptions with cytoplasmic membrane. J. Cell Sci. 113, 1891–1902 (2000).
9. Togo, T. Disruption of the plasma membrane stimulates rearrangement of microtubules and lipid traffic toward the wound site. J. Cell Sci. 119, 2780-2786 (2006).
10. Hoffman, J. F. On red blood cells, hemolysis and resealed ghosts. Adv. Exp. Med. Biol. 326, 1–15 (1992).
11. McNeil, P. L., Miyake, K., Vogel, S. S. The endomembrane requirement for cell surface repair. Proc. Natl Acad. Sci. USA 100, 4592–4597 (2003).
12. Freedman, J. C. et al. Membrane potential and the cytotoxic Ca cascade of human red blood cells. Soc. Gen. Physiol. Ser. 43, 217–231 (1988).
13. Togo, T., Krasieva, T. B., Steinhardt, R. A. A decrease in membrane tension precedes successful cell-membrane repair. Mol. Biol. Cell 11, 4339–4346 (2000).
14. Sheetz, M. P. Cell control by membrane–cytoskeleton adhesion. Nature Rev. Mol. Cell Biol. 2, 392–396 (2001)
15. McNeil ,P. L., Kirchhausen, T. An emergency response team for membrane repair. Nature Reviews Molecular Cell Biology 6, 499-505 (June 2005)
16. Retterer ST, Melechko A, Hensley DK, Simpson ML, Doktycz MJ. Positional control of catalyst nanoparticles for the synthesis of high density carbon nanofiber arrays. Carbon N Y.;46(11):1378-1383 (2008)
17. McKnight TE, Ericson MN, Jones SW, Melechko AV, Simpson ML. Vertically Aligned Carbon Nanofiber Arrays: An Electrical and Genetic Substrate for Tissue Scaffolding. Conf Proc IEEE Eng Med Biol Soc. 5381-3 (2007)
18. McKnight, TE, Melechko, AV, Griffin, GD, Guillorn, MA, Merkulov, VI, Serna, F., Hensley, DK, Doktycz, MJ, Lowndes, DH, Simpson, ML. Intracellular integration of synthetic nanostructures with viable cells for controlled biochemical manipulation. Nanotechnology 14 551-556 (2003)

18. Belkacemi, L., Bédard, I., Simoneau, L., Lafond, J**.** Calcium channels, transporters and exchangers in placenta: a review. J. Sci. Dir. 37, 1-8 (2005)
19. Benjamini, Y., Hochberg, Y. Controlling the false discovery rate: a practical and powerful approach to multiple testing. Journal of the Royal Statistical Society, Series B (Methodological) **57** (1): 289–300 (1995)

VITA

Sebastian Morgan Harris

Candidate for the Degree of

Master of Science

Thesis: MICROARRAY TIME COURSE ASSAYS OF CHO-CELLS IMPALED ON VERTICALLY ARRAYED NANOFIBERS

Major Field: Biochemistry and Molecular Biology

Biographical:

Education:
Completed the requirements for the Master of Science in Biochemistry and Molecular Biology at Oklahoma State University, Stillwater, Oklahoma in December, 2009.
Completed the requirements for the Bachelors of Science in Chemistry (ACS Certified) at Southwestern Oklahoma State University, Weatherford, Oklahoma in May, 2007.

Experience: Research Assistant (2007-2009) for Dr. Peter Hoyt at Oklahoma State University, Stillwater, Oklahoma
Teaching Assistant (2007-2009) for Dr. Sharon Ford & Dr. Benjamin Sandler at Oklahoma State University, Stillwater, Oklahoma

Professional Memberships: American Association for the Advancement of Science (AAAS)

Name: Sebastian Morgan Harris Date of Degree: December, 2009

Institution: Oklahoma State University Location: Stillwater, Oklahoma

Title of Study: MICROARRAY TIME COURSE ASSAYS OF CHO-CELLS IMPALED ON VERTICALLY ARRAYED NANOFIBERS

Pages in Study: 42 Candidate for the Degree of Master of Science

Major Field: Biochemistry and Molecular Biology

Scope and Method of Study:

Cells impaled onto nanofibers may be used as gene delivery devices to regulate expression of impaled cells, and to influence the cell-cell interactions of surrounding cells. To use this novel technology, it is essential to identify a time point following impalement where exogenous gene expression can be precisely monitored. RNA was extracted from CHO-cells impaled on vertically array nanofibers isolated over a series of time points ending at 24 hours. After fluorescent labeling, the RNA is hybridized to mouse microarray slides. Differential expression data was analyzed using Array Studio from Omicsoft. Functional annotation of the differentially expressed genes was performed using bioinformatics software including Genesis from Graz University of Technology, KEGG from Kanehisa Laboratories, and Web Gestalt from Vanderbilt University.

Findings and Conclusions:

Previous observations of membrane repair in response to wounding included reorganization of cytoskeleton and deployment of vesicles to the plasma membrane. Our data suggested that these mechanisms persisted up to four hours following impalement and membrane perturbation. Novel observations made were constant glycan activity, heparan sulfate, as a potential sealing factor, and over expression of G-protein coupled receptors labeled as Olfactory receptors. Surprisingly, induction of apoptosis was not detected during 24 hours. Finally, all observations show that by 24 hours differential expression has returned to nominal levels in comparison to control. This final key observation resolves a past criticism of a potentially very noisy expression background when conducting transfection experiments using plasmid linked nanofibers as the delivery method.